

# UStyle: Waterbody Style Transfer of Underwater Scenes by Depth-Guided Feature Synthesis

Md Abu Bakr Siddique, Vaishnav Ramesh, Junliang Liu, Piyush Singh,  
and Md Jahidul Islam

RoboPI Laboratory, Department of ECE, University of Florida

## Abstract

The concept of *waterbody style* transfer remains largely unexplored in the underwater imaging and vision literature. Traditional image style transfer (STx) methods primarily focus on artistic and photorealistic blending, often failing to preserve object and scene geometry in images captured in high-scattering mediums such as underwater. The wavelength-dependent nonlinear attenuation and depth-dependent backscattering artifacts further complicate learning underwater image STx from unpaired data. This paper introduces UStyle, the first data-driven learning framework for transferring waterbody styles across underwater images without requiring prior reference images or scene information. We propose a novel depth-aware whitening and coloring transform (**DA-WCT**) mechanism that integrates physics-based waterbody synthesis to ensure perceptually consistent stylization while preserving scene structure. To enhance style transfer quality, we incorporate carefully designed loss functions that guide UStyle to maintain colorfulness, lightness, structural integrity, and frequency-domain characteristics, as well as high-level content in VGG and CLIP (contrastive language-image pretraining) feature spaces. By addressing domain-specific challenges, UStyle provides a robust framework for no-reference underwater image STx, surpassing state-of-the-art (SOTA) methods that rely solely on end-to-end reconstruction loss. Furthermore, we introduce the **UF7D dataset**, a curated collection of high-resolution underwater images spanning seven distinct waterbody styles, establishing a benchmark to support future research in underwater image STx. The UStyle inference pipeline and UF7D dataset is released at: <https://github.com/uf-robopi/UStyle>.

## Index Terms

Style Transfer; Waterbody Fusion; Underwater Imaging; Underwater Vision.

## I. INTRODUCTION

Image style transfer (STx) in underwater imagery has significant potential in data augmentation, robotic vision, photometry, and imaging technologies [1]. Traditional neural style transfer (NSTx) approaches [2], [3] primarily focus on terrestrial imagery, aiming to transfer artistic or photometric features across images. However, the concept of “**waterbody style**” transfer presents a distinct challenge [1], where the goal is to generate an underwater image in the style of a different aquatic environment while preserving the structural integrity of the scene. Although unpaired images from various waterbodies can be collected, conventional NSTx techniques—optimized for perceptual photorealism [4] or artistic blending [5], [6], [7]—struggle to accommodate the unique distortions introduced by underwater light absorption and scattering [8]. As a result, these methods often produce unnatural style adaptation and significant structural loss.

Currently, no learning-based frameworks exist for waterbody STx in underwater imagery. Our previous work, AquaFuse [1], introduced a physics-based approach for *waterbody fusion*, facilitating data augmentation across different aquatic environments. However, this method relies on a closed-form formulation that requires a carefully selected, noise-free reference image and prior scene information,

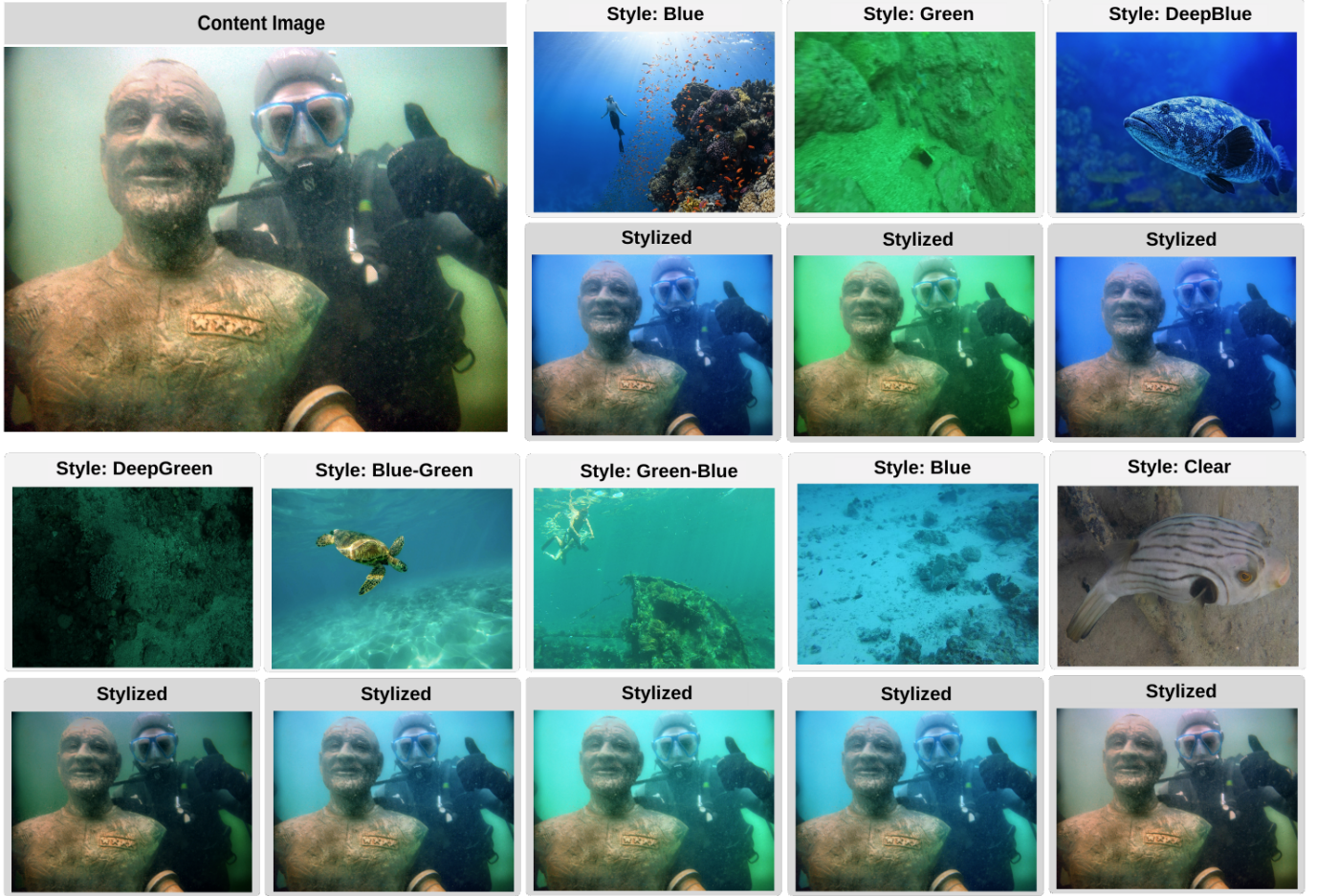


Fig. 1: Visualizations of the underwater image STx capabilities of UStyle are shown. The content image (top left) is transformed into different *waterbody* styles. For any given style image, note that its waterbody characteristics are transferred to the content scene, while its object geometry and structural details of the content image remain preserved. Such no-reference waterbody fusion is useful as a geometry-preserving data augmentation tool in underwater imaging, photometry, and robotics applications.

including depth, incident angle, and attenuation parameters. Consequently, leveraging large-scale vision-based learning models for robust underwater STx without explicit reference images or prior information remains a challenge. Recent advancements in NST [4], [7] and vision-language models [9], [10] present an opportunity to address this gap. However, developing a learning-driven approach capable of accurately adapting underwater distortions while preserving structural details remains an unexplored area of research.

In this paper, we propose **UStyle**, the first data-driven learning pipeline for waterbody STx in underwater imagery. We present the model architecture, choice of loss functions, and the training strategy required to address the limitations of existing NSTx pipelines for underwater STx. Specifically, UStyle integrates a residual encoder-decoder to extract local structural details at different spatial resolutions while leveraging a progressive multi-stage training strategy to refine waterbody feature learning by domain-specific loss functions. Moreover, to guide the stylization process, we use a physics-based method [1] to synthesize the waterbody from the style image by following the state-of-the-art (SOTA) underwater image formation model [8]. This synthesized *waterbody style* is then fused by a novel depth-guided whitening and coloring transform (**DA-WCT**) mechanism, which makes sure that no object/scene information is transferred to the content image. A few sample examples are illustrated in Fig. 1.

For comprehensive evaluation, we compile an underwater dataset named **UF7D** – featuring 4,050 high-resolution images with paired depth annotations across seven different waterbody styles: Blue (B), Green (G), Deep Blue (DB), Deep Green (DG), Clear (C), Blue-Green (B-G), and Green-Blue (G-B). It enables data-driven learning for underwater STx, allowing the model to generalize across diverse aquatic environments with varying optical properties. Most images are sourced from existing SOTA databases [11], [12], [13], [14], [15] for imaging, object detection, image enhancement, and robotics applications; thus, it serves as a useful benchmark for future research. To this end, we conducted a thorough benchmark evaluation of underwater STx, by comparing UStyle with several SOTA methods named StyTR-2 [7], MCCNet [16], ASTMAN [17], IEContraAST [5], PhotoWCT2 [4], and AquaFuse [1].

The key contributions of this work are summarized below:

- 1) **Underwater STx learning pipeline and dataset:** UStyle is the first data-driven STx framework for underwater scenes, eliminating the need for explicit scene priors required by physics-based STx models [1]. Instead of relying on carefully selected reference images and waterbody parameters, UStyle employs a learning-based STx approach that robustly adapts to diverse aquatic environments with varying waterbodies. We also introduce the UF7D dataset, a comprehensive collection of 4,050 high-resolution underwater images of waterbody styles, which supports supervised training and benchmark evaluation across varying underwater conditions.
- 2) **Novel contributions in UStyle:** We design and develop UStyle to (learn to) blend image features while being aware of the object geometry in underwater scenes for waterbody STx. Our proposed architecture (a) integrates a ResNet-based [18] encoder-decoder with hierarchical skip connections [19] for effective multi-scale feature fusion; (b) employs a progressive multi-stage training strategy [20] for stabilized style-content blending; and (c) domain-specific loss functions learn image statistics (color, lightness) [21], structural details (SSIM [22], FFT [23]) and high-level image contents (VGG [24], CLIP [25]). This guided training strategy is leveraged by our proposed DA-WCT mechanism for depth-aware waterbody stylization, ensuring perceptual fidelity and geometric consistency.
- 3) **SOTA performance and benchmark evaluation:** We conduct comprehensive experimental evaluations validating that UStyle consistently outperforms leading STx methods—such as StyTR-2 [7], MCCNet [16], ASTMAN [17], IEContraAST [5], and PhotoWCT2 [4]—across key metrics such as PSNR, SSIM, RMSE, and LPIPS. Ablation studies also reveal that our proposed DA-WCT mechanism and domain-specific loss functions can deal with the underwater image distortions to generate perceptually coherent stylization. We also compare the performance with physics-based approaches—such as AquaFuse [1]—to validate that UStyle-generated images preserve the structural contents of the scene while fusing waterbody styles. These results establish UStyle as a robust and effective solution for no-reference underwater image STx applications.

UStyle provides a robust and efficient solution for no-reference underwater STx, addressing the limitations of traditional artistic and photorealistic STx approaches. Its ability to preserve geometric consistency while achieving realistic waterbody transformations makes it an ideal framework for real-world marine robotics and imaging applications. UStyle opens up significant opportunities for further research in real-time video-based stylization, data augmentation, and interactive augmented and virtual reality (AR/VR) domains.

## II. BACKGROUND AND RELATED WORK

Image style transfer (STx) techniques blend the *content* of one image with the *style* of another [26], [27], [28], unlocking a wide array of applications across computer vision, virtual reality, robotics, and digital art creation. We can group current advancements in STx into critical domains such as artistic, photorealistic, non-photorealistic, semantic, and multimodal techniques. Each category uses its methods to improve the

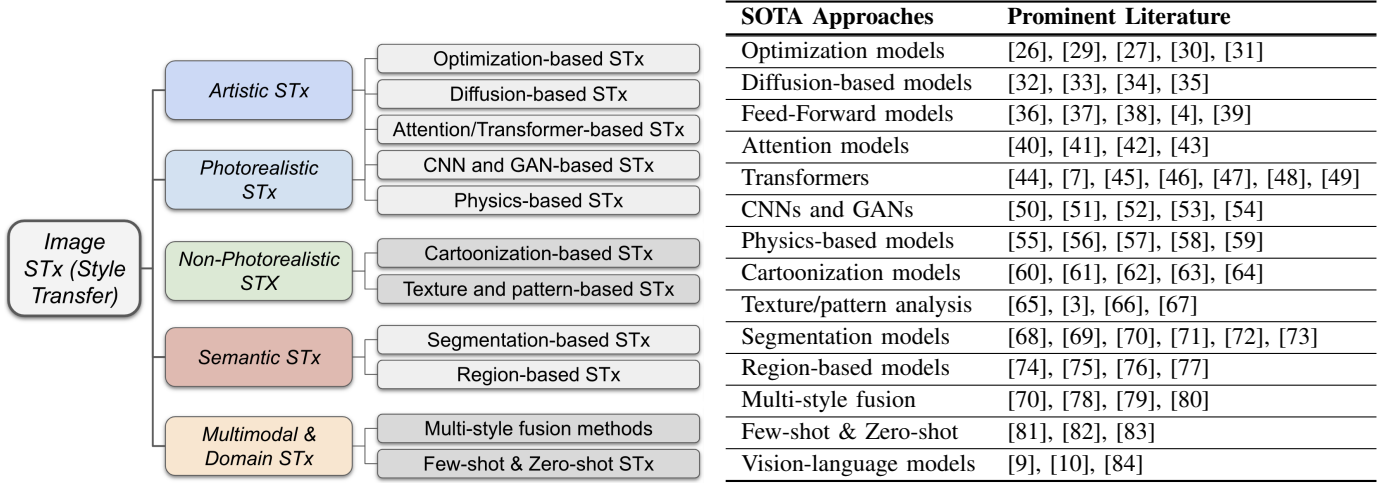


Fig. 2: A snapshot of the SOTA literature on image-based style transfer (STx) approaches.

adaptability and realism of STx, such as optimization algorithms, feed-forward architectures, attention mechanisms, and transformers (see Fig. 2). These approaches collectively push the boundaries of what is achievable in image synthesis, making it possible to preserve structure, adapt to high-resolution outputs, and achieve detailed, context-aware stylization.

#### A. Artistic and Non-Photorealistic Style Transfer

Artistic STx aims to apply one image’s artistic characteristics, such as brushstrokes, textures, or color palettes, to another image’s content. Following the seminal work by Gatys *et al.* [85], many deep visual learning-based networks have been proposed [36], [37], [38]. In particular, Johnson *et al.* [86] and Ulyanov *et al.* [87] develop feed-forward networks that apply predefined styles in real-time, making the process much faster. One limitation of their approach is that their network needs to be trained for a specific style. Huang and Belongie [36] address this issue with adaptive instance normalization (AdaIN). AdaIN adjusts the mean and variance of content features to match style features, enabling the transfer of arbitrary styles [88], [89], [90]. Li *et al.* [37] introduce the whitening and coloring transform (WCT), which applies a *whitening* operation to remove content, followed by a *coloring* operation to inject style statistics.

Non-photorealistic rendering (NPR) methods are a superset of artistic STx, focusing on cartooning, sketches, and more abstract art. Early work in this domain is grounded in traditional computer graphics with handcrafted filters and procedural algorithms, whereas recent work uses deep learning techniques to achieve more sophisticated stylizations. Zhao *et al.* [60] introduces a GAN-based approach for high-quality image cartoonization, capturing stylistic nuances with remarkable fidelity. Ahn *et al.* [61] develop an interactive framework that allows users to influence the stylization in real-time, enhancing creativity and personalization. Chen *et al.* [62] proposes DecoGAN, enabling controllable decoration and stylization of images with user inputs. Additionally, techniques such as language-guided STx [65], fast neural doodling [3], and style consistency models [66] expand the possibilities of NPR, making sophisticated stylization accessible to a broader audience. Kim *et al.* [67] focuses on texture and pattern analysis to preserve fine-grained details during STx, resulting in more cohesive and visually appealing images. These advancements collectively push the boundaries of NPR, enabling the creation of diverse and artistically rich images through deep learning techniques.

Various *attention* mechanisms have enhanced artistic STx in recent years by capturing complex relationships between content and style. For instance, self-attention GANs [40] enables different parts of an



image to interact more effectively to enhance spatial awareness in the artistic rendering process. Building on this, style-attention networks (SANet) [41] achieve more precise style adjustments in different image areas for refined artistic control. These advancements help balance global and local features, improving the quality of fine-grained stylization and overall composition.

### B. Photorealistic Style Transfer

Photorealistic STx applies stylistic changes while keeping the realism and structure of the original image intact. This is essential in understanding visual scenes and robotics applications. Early methods like deep photo style transfer (DPST) [29] use optimization techniques to achieve photorealism, although they struggle with high-resolution input images. To address this, Li *et al.* introduces PhotoWCT [38], which uses cascaded autoencoders to transform content features while keeping structural details intact. PhotoWCT2 [4] improves this by reducing parameters with blockwise training for faster stylization of high-resolution images. Wavelet-based WCT2 [39] uses wavelet pooling and un-pooling layers to preserve fine details during the STx process better.

Beyond feed-forward models, vision transformers excel at modeling long-range dependencies and spatial coherence, making them ideal for tasks where preserving local details and global structure is essential. StyTr2 by Deng *et al.* [7] is a prominent work that employs dual transformer encoders: one each for content and style; it introduces the idea of content-aware positional encoding (CAPE) to ensure scale invariance and spatial preservation. Contemporary works also explore unsupervised STx learning, with models like TransGAN [50], integrating transformers with GANs. More advanced attention mechanisms such as transformer-in-transformer (TNT) [48] further enhance STx by capturing complex dependencies through a nested architecture. Recent developments in diffusion-based models [32], [35] demonstrate further improvements by disentangling style and content for controlled (localized) adjustments.

On the other hand, physics-based methods use precise rendering to improve *photorealism*. For instance, Monte Carlo ray tracing simulates realistic lighting and shading to capture natural light interactions. Bidirectional reflectance distribution function (BRDF) modeling [57] preserves material properties like glossiness and roughness for more realistic appearance. These models consider how light reflects off surfaces to capture various light-material interactions. Another notable approach is deep image prior (DIP) [56], which uses a neural network to learn photorealism directly from the input image. It leverages natural image priors ( e.g., smooth regions, sharp edges) to handle tasks such as denoising, restoration, and style transfer. Moreover, retinex theory [91] powers many algorithms to improve photorealism by exploiting the geometry of how the human eye separates light from surface reflectance. Techniques like multi-scale retinex [92] restore true colors by ensuring natural color balance and contrast. Inverse tone mapping techniques [55] focus on rendering high-dynamic-range images, whereas optical flow-based STx [58] maintain spatial coherence to ensure smooth transitions in motion, shading, and texture gradients.

### C. Semantic and Multimodal Style Transfer

Semantic STx integrates a high-level understanding of image content to apply styles context-awarely, enhancing the coherence between the transferred style and the underlying content. For instance, Wang *et al.* [72] employs the SOTA semantic segmentation model DeepLab [71] to preserve object boundaries during STx. Lin *et al.* [68] further refine this approach by leveraging segmentation to maintain structural details, ensuring context-aware consistent STx. On the other hand, region-based models focus on selectively transferring styles to specific areas within an image. Niu *et al.* [74] propose a region-adaptive STx method that applies styles to distinct regions based on their semantic relevance. Liao *et al.* [77] develop a semantic-guided attention mechanism to enhance stylization in targeted regions, improving aesthetic quality and

content preservation. These approaches allow for more precise control over the stylization process by fusing global semantic context and local features for improved STx.

Multimodal STx extends these concepts by incorporating additional modalities, such as depth information or textual descriptions, to guide the stylization. Ye *et al.* [70] explores multimodal learning techniques to fuse visual and textual data, enabling more expressive and versatile STx. Zheng *et al.* [69] applies retinal image segmentation combined with STx for medical imaging applications, demonstrating the versatility of multimodal approaches. Besides, few-shot and zero-shot learning techniques have been introduced to address the challenge of limited-style exemplars. Fu *et al.* [81] present StyleAdv, a few-shot adversarial learning framework that can adapt to new styles with minimal data. Huang *et al.* [82] proposes a zero-shot STx method using residual decay networks, eliminating the need for style images during training. Liu *et al.* [83] introduce StyleRF, which leverages neural radiance fields for zero-shot STx, enabling the application of novel styles without prior exposure.

Vision-language models (VLMs), particularly Contrastive Language–Image Pre-training (CLIP), enable the integration of textual and visual information for advanced image processing tasks [84]. Their robust image encoders capture comprehensive representations of image features, enhancing the potential for applications such as image STx. Clipstyler [9] framework achieves image STx solely from text descriptions by leveraging a patch-wise CLIP loss and perspective augmentation, thus eliminating the need for reference (style) images. Yang *et al.* [10] propose a zero-shot contrastive loss for diffusion models [33] that leverage patch-wise contrastive learning to preserve semantic content during text-guided STx without additional fine-tuning or auxiliary networks. These advancements significantly enhance the flexibility and scalability of STx models, making them more practical for real-world applications.

#### D. Underwater Domain Style Transfer

Traditionally, *domain STx* methods are used to model underwater image distortions for synthetic data generation [93], [94]; the stylized distorted pairs are then used for learning image enhancement [95], [11] or improved object detection [15], [96]. These models enhance color correction, clarity, and stylization in a unified learning pipeline by separating content and style across different domains. For instance, Chen *et al.* [47] introduces a domain adaptation framework that leverages transformers for image enhancement [97], [98]. Zhou *et al.* [99] uses a transformer-based STx model for stylized representation learning of target recognition in underwater acoustic imagery. Our previous work AquaFuse [1] proposes a physics-guided method for geometry-preserving waterbody fusion for photometric data augmentation, which requires a prior reference image and known waterbody parameters. This work explores no-reference image STx from comprehensive multimodal learning databases – for the first time in the literature.

### III. UF7D DATASET

#### A. Data Preparation and Categorization

To enable data-driven learning of no-reference waterbody STx, we compile a comprehensive collection of high-resolution underwater image database named **UF7D**. It includes 7 style categories: Blue (B), Blue-Green (B-G), Clear (C), Deep Blue (DB), Deep Green (DG), Green (G), and Green-Blue (G-B). A few samples for each category are shown in Figure 3.

A key feature of UF7D dataset is that it includes the scene depth maps for each image, generated by using the *DepthAnything V2* model [100]. With high-resolution images and depth information, the UF7D dataset supports deep visual learning applications such as underwater image style transfer, enhancement, object detection, and more. To this end, our data collection process focused on the following aspects:

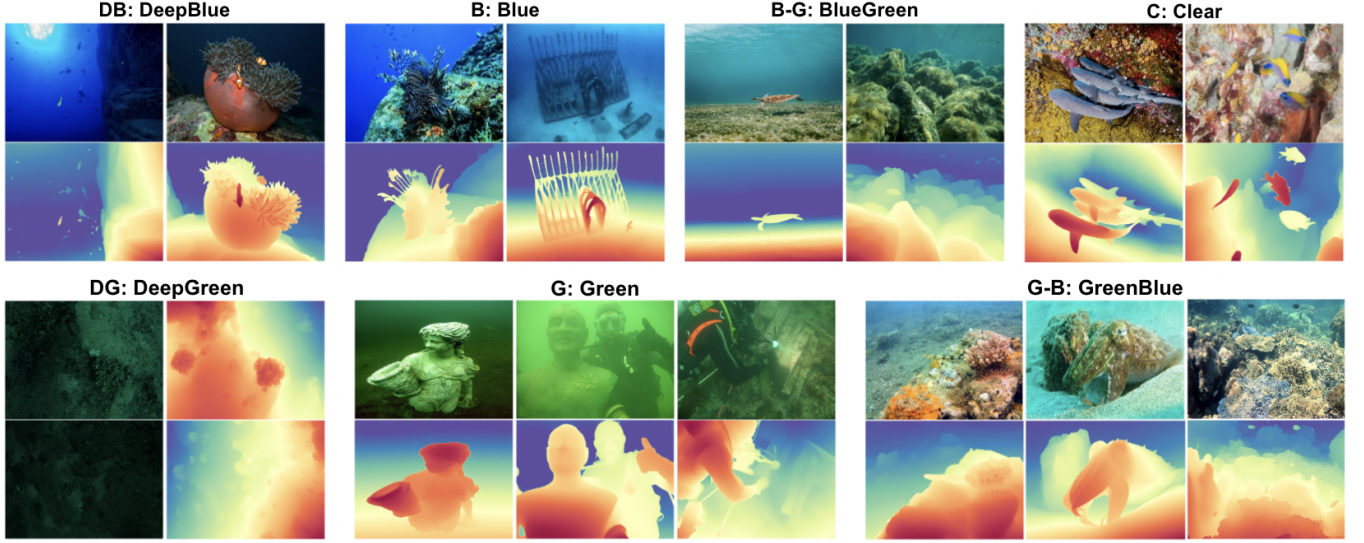
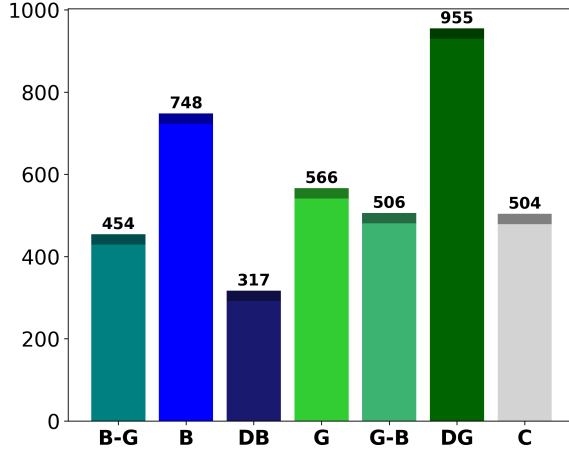


Fig. 3: A few samples from the UF7D dataset are shown for each of its seven style categories.



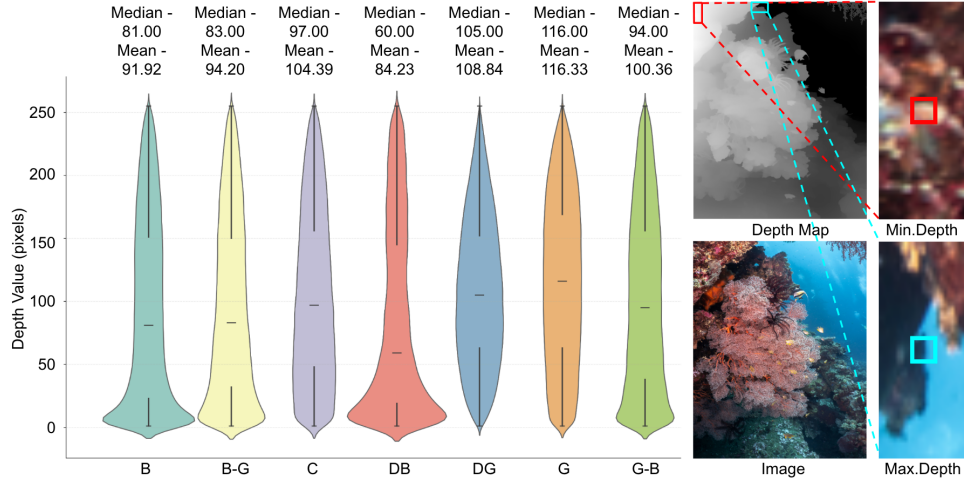
(a) Distribution of images for all categories.

| Resolution        | # of Images |
|-------------------|-------------|
| 640 × 480         | 1633        |
| Up to 800 × 600   | 56          |
| Up to 1024 × 768  | 106         |
| Up to 1280 × 720  | 111         |
| Up to 1920 × 1080 | 374         |
| Above 1920 × 1080 | 1770        |
| Total # of Images | <b>4050</b> |

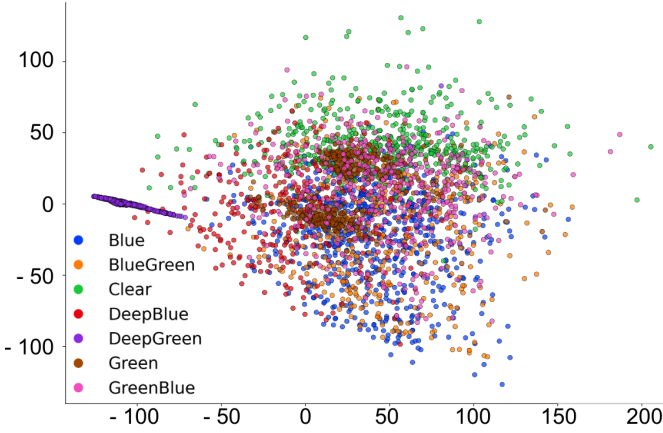
(b) Image resolution information.

Fig. 4: An overview of the UF7D dataset: it has a balanced distribution of seven waterbody style categories, each consisting of high-resolution natural underwater images.

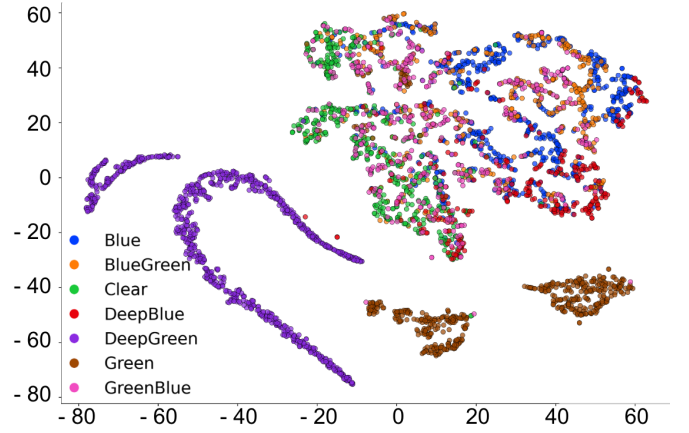
- 1) **Scene Diversity:** UF7D includes a wide variety of natural underwater scenes that are sourced from various benchmark image databases [11], [12], [13], [101], [14], [15] and other public platforms such as Unsplash [102] and Flickr [103]. Our collection spans various objects including coral reefs, shipwrecks, pipelines, and various marine species (fish, plants, rocks) – enabling robust data-driven learning across diverse underwater conditions [104], [105].
- 2) **Image Quality:** UF7D has a total of 4,050 images, over 44% of which are above 1920 × 1080 resolution (see Fig. 4), offering high-resolution image contents necessary for fine-grained analyses.
- 3) **Balanced STx Categories:** We relied on human visual perception for curating and compiling the seven style categories. As shown in Figure 4a, these categories are evenly represented across the dataset, comprising the spectrum of dark blue to dark green colors, as well as clear images.



(a) Violin plots showing depth value distributions across all categories. A particular example of depth variation is shown on the right; the blue box highlights a background region and the red box indicates a foreground region.



(b) PCA projection of global color characteristics (with 92% variance captured in first two components).



(c) t-SNE visualization of local color statistics; the clusters validate the human-perceived category distinctions.

Fig. 5: Statistical analyses and relevant information on the UF7D dataset.

## B. Dataset Statistics and Analyses

Our statistical analysis reveals that UF7D consists of comprehensive coverage of varying underwater depths. Figure 5a illustrates the depth distributions by violin plots, where width represents the frequency density at each depth level. Here, we make the following observations.

- **Cross-category Variation:** Median depths range from 60 to 116 pixels across categories, with Green (G) environments showing the highest median and Deep Blue (DB) the lowest.
- **Within-category Distribution:** Categories exhibit distinct depth patterns; for instance, Clear (C) waters show consistent depth profiles, while Deep Blue (DB) shows a much wider variance.

We further perform detailed statistical analysis to validate our human-perceived style categorization process. Figure 5 presents the following two complementary analyses:

- **Global Color Structure:** Principle component analysis (PCA) reveals distinct clustering patterns for all categories, with the first two principal components capturing 92% of total color variance; see Figure 5b. The primary component embeds 76% variance, effectively separating blue-dominated waters from green-dominated waters, which is consistent with our human perceptual evaluations.



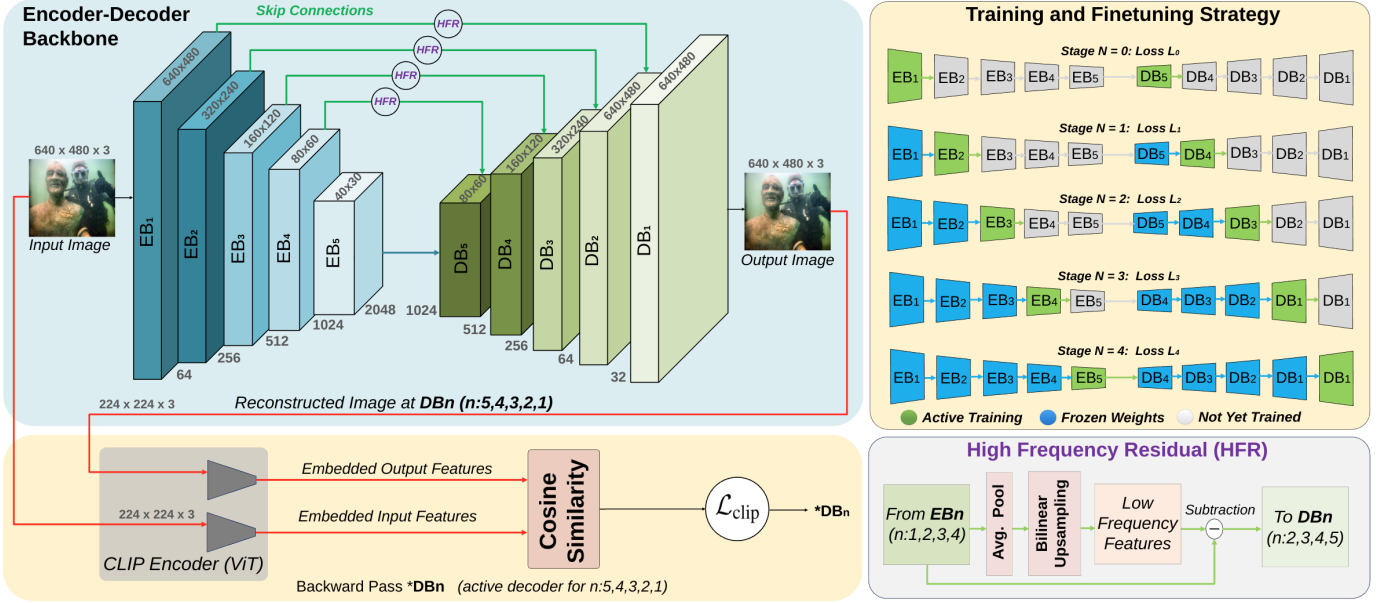


Fig. 6: Overview of our UStyle model, featuring an encoder-decoder backbone with skip connections, high-frequency residual (HFR) paths, and a CLIP-based coarse similarity module for aligning intermediate features with semantic cues. A multi-stage learning strategy is adopted that progressively trains deeper symmetric blocks to preserve both coarse structure and fine details in the waterbody fusion process.

- **Local Color Relationships:** A t-SNE (t-distributed stochastic neighbor embedding) visualization demonstrates clear separations among the style categories; see Figure 5c. This confirms that images within each category share consistent spatial color characteristics.

These analyses validate that our waterbody style categorization based on human perception is statistically consistent as well. The inter-category and intra-category statistics also suggest that the underlying *style* can potentially be learned with tailored training strategies.

#### IV. USTYLE MODEL & LEARNING PIPELINE

We present **UStyle**, a novel waterbody style transfer framework that integrates a deep encoder-decoder architecture, progressive blockwise training, and a depth-aware stylization module. Given a content image  $I_c \in \mathbb{R}^{H \times W \times 3}$  and a style image  $I_s \in \mathbb{R}^{H \times W \times 3}$ , UStyle generates a stylized output  $I_{cs}$  by fusing waterbody characteristics from the style image while preserving scene geometry of the content image. The depth maps  $D_s$  and  $D_c$ , representing the depth information of the style and content images, respectively, adapt features based on depth.  $D_s$  guides the extraction of waterbody details from the style image, while  $D_c$  ensures content-aware stylization by preserving structural consistency and depth-dependent variations during style transfer. As shown in Fig. 6, the UStyle learning pipeline comprises three major components: (1) an encoder-decoder backbone for multi-scale feature extraction with fine spatial details and high-level semantics; (2) a progressive training strategy for stable coarse-to-fine stylization; and (3) a depth-aware stylization module for effective waterbody style transfer.

##### A. Encoder-Decoder Backbone

We use a ResNet50 [18] encoder ( $\mathcal{E}$ ) partitioned into five sequential blocks  $EB_{1:5}$ , which extract increasingly finer features  $\{F_{i,c}\}_{i=0:4}$  and  $\{F_{i,s}\}_{i=0:4}$  from a given content and style images, respectively. These feature maps are then fed into a decoder  $\mathcal{D}$  with hierarchical ( $EB_{i-1} \rightarrow DB_i$ ) skip connections.

The symmetric skip connections retain spatial structures and propagate high-frequency details from the encoder to the decoder. Each decoder block  $DB_i$  consists of a transposed convolution [106] for upsampling, followed by a convolutional layer [107], batch normalization [108], and a ReLU activation [109]. Rather than explicitly computing residuals via average pooling and subtraction, our design preserves these details through the original skip connections. These features are fused to achieve waterbody STx with pixel-wise guidance from the content depth map  $D_c$ , ensuring that the fused features  $F_{i,cs}$  adapt to both structural (object geometry) and stylistic (waterbody) elements. This fusion is performed by our novel depth-aware stylization module; see Section IV-C.

### B. Progressive Pre-Training and Domain-specific Finetuning

We implement a sequential blockwise approach in UStyle, where the encoder-decoder network is optimized progressively over five stages ( $N = 1:5$ ). Completed  $EB_i - DB_i$  blocks are frozen to ensure stability of the training, as shown in Fig. 6. Initially, the model is pre-trained on a large-scale atmospheric dataset (MSCOCO-2017 [110]) with a weighted combination of reconstruction loss [111], feature reconstruction loss [86], and perceptual loss. During the training of the first stage ( $N = 0$ ), the network is optimized using only a reconstruction loss  $\mathcal{L}_r = \|\mathbf{I}_c - \hat{\mathbf{I}}_c\|_2^2$  where  $\hat{\mathbf{I}}_c$  denotes the decoder's output. In subsequent stages ( $N > 0$ ), additional losses are introduced to ensure feature-level consistency and perceptual fidelity. These include a feature reconstruction loss  $\mathcal{L}_{feat} = \|\mathbf{F}_i - \hat{\mathbf{F}}_i\|_2^2$  and a perceptual loss  $\mathcal{L}_{percept} = \|\phi(\mathbf{I}_c) - \phi(\hat{\mathbf{I}}_c)\|_2^2$ , where  $\phi(\cdot)$  is a high-level feature extractor based on VGG-16 [24].

After pretraining, UStyle is fine-tuned on a large-scale underwater dataset (USOD10K [112]) for domain-specific supervision with SSIM loss  $\mathcal{L}_{ssim} = 1 - SSIM(\mathbf{I}_c, \hat{\mathbf{I}}_c)$ , color consistency loss in LAB image space  $\mathcal{L}_{color} = \|\text{LAB}(\mathbf{I}_c) - \text{LAB}(\hat{\mathbf{I}}_c)\|_2^2$ , and frequency-domain loss by Fast Fourier Transforms (FFT)  $\mathcal{L}_{fft} = \|\mathcal{F}(\mathbf{I}_c) - \mathcal{F}(\hat{\mathbf{I}}_c)\|_2^2$ . Moreover, CLIP-based content supervision is incorporated by introducing a CLIP loss [25] to ensure semantic alignment. It is defined as:

$$\mathcal{L}_{clip} = 1 - \text{cosine\_similarity}(\text{CLIP}(\mathbf{I}_c), \text{CLIP}(\hat{\mathbf{I}}_c)). \quad (1)$$

The overall objective functions for multi-stage training are as follows:

$$\mathcal{L}_0 = \mathcal{L}_r + \mathcal{L}_{ssim} + \mathcal{L}_{color} + \mathcal{L}_{fft} + \mathcal{L}_{clip} \quad (N = 0) \quad (2)$$

$$\mathcal{L}_N = \mathcal{L}_r + \mathcal{L}_{ssim} + \mathcal{L}_{color} + \mathcal{L}_{fft} + \mathcal{L}_{clip} + \mathcal{L}_{feat} + \mathcal{L}_{percept} \quad (N = 1, 2, 3, 4) \quad (3)$$

This progressive training approach allows the network to learn robust multi-scale feature representations while ensuring content, style, and depth consistency for high-fidelity underwater waterbody style transfer.

### C. Depth-aware Stylization

We design a depth-aware stylization function: **DA-WCT** which extends the multi-scale blending concept from the WCT (whitening and coloring transform) literature [37]. DA-WCT integrates a physics-guided waterbody estimation method for depth-guided feature blending via WCT. First, we estimate the *waterbody* from the style image  $\mathbf{I}_s$  using a physics-guided method [1]; from its depth map  $D_s$ , we leverage the 5% farthest pixels' median values to estimate the waterbody background in  $\mathbf{I}_s$ . A color filter is then applied to retain only bluish-green pixels, removing red-channel influence due to differential light attenuation underwater. The extracted waterbody  $\mathbf{B}_s$  is then fed into the encoder to obtain the style features.

Let  $F_c$  and  $F_s$  denote the content and style feature maps extracted from the encoder, respectively. We first perform a WCT-based stylization to align the statistics of  $F_c$  with those of  $F_s$ ; the stylized feature  $\tilde{F}_{cs}$  is computed as  $\tilde{F}_{cs} = \mu_s + C_s^{1/2} C_c^{-1/2} (F_c - \mu_c)$ , with  $\mu_c, \mu_s$  being the channel-wise means and

$C_c, C_s$  the covariance matrices of  $F_c$  and  $F_s$ , respectively. Let  $\mathbf{D}_c$  denote the single-channel content depth map, a global depth threshold  $\tau \in [0, 1]$  is computed using Otsu’s method [113]. Next, an adaptive scaling factor  $k$  is derived by first smoothing  $\mathbf{D}_c$  via average pooling with a  $5 \times 5$  kernel, then computing the global mean and standard deviation as follows:

$$\mu_d = \frac{1}{H \cdot W} \sum_x \text{avgpool}(\mathbf{D}_c(x)) \quad (4)$$

$$\sigma_d = \sqrt{\frac{1}{H \cdot W} \sum_x \left( \text{avgpool}(\mathbf{D}_c(x)) - \mu_d \right)^2} \quad (5)$$

With the tunable scaling factors  $\tau$  and  $k$  determined, the depth weight map for each pixel is computed using the sigmoid function.

$$w(x) = \sigma\left(-k \cdot (\mathbf{D}_c(x) - \tau)\right) = \frac{1}{1 + \exp\left(k \cdot (\mathbf{D}_c(x) - \tau)\right)} \quad (6)$$

Subsequently, the blended feature is obtained by merging the stylized features  $\tilde{F}_{cs}(x)$  with the original content features  $F_c(x)$  as follows

$$F_{\text{depth}}(x) = w(x) \cdot \tilde{F}_{cs}(x) + [1 - w(x)] \cdot F_c(x) \quad (7)$$

In our formulation, pixels with higher depth values (*i.e.*, farther objects) yield  $w(x) \rightarrow 1$  and favor the stylized features  $\tilde{F}_{cs}(x)$ . In contrast, pixels with lower depth values get  $w(x) \rightarrow 0$ , preserving more of the original content features  $F_c(x)$ . A global style strength parameter  $\alpha \in [0, 1]$  is applied to control the *degree* of the underlying stylization process.

$$F_{cs} = \alpha F_{\text{depth}} + (1 - \alpha) F_c. \quad (8)$$

Furthermore, to capture both global and local style characteristics, our DA-WCT function is applied at multiple scales  $s \in \{1.0, 0.75, 0.5, 0.25\}$ , with the fused features at each scale, to obtain multi-scale features  $F_{\text{multi}}$ . At each scale (stage) of the decoder, these *fused features* replace the corresponding *content features* with multi-scale fusion. The stylized image is then constructed from the decoder  $\mathcal{D}$  as  $\mathbf{I}_{cs} = \mathcal{D}(F_{\text{multi}})$ . Finally, a guided filter named GIF smoothing [114] is applied as a post-processing step to enhance the visual consistency of the final output image.

$$\mathbf{I}_{\text{stylized}} = \text{GIF}(\mathbf{I}_{cs}) = \text{GIF}(\mathcal{D}(F_{\text{multi}})). \quad (9)$$

**Implementation Details.** UStyle is implemented in PyTorch with OpenCV and Torch libraries. We use Adam optimizer with an initial learning rate of  $10^{-4}$  for the supervised learning. Training is conducted on a Linux system equipped with 4 GPUs and 32 GB of RAM. At the first stage of training, the encoder-decoder network is pre-trained on the MSCOCO-2017 with 118K training samples for 10 epochs. It is then fine-tuned on USOD10K underwater dataset with 10K examples for another 10 epochs. The whole training and fine-tuning takes 82 hours to complete. Once trained, the frozen graph is used for inference, executed on a single GPU and 16 GB of RAM.

**Inference Pipeline.** The inference process of UStyle follows a structured pipeline to achieve high-fidelity underwater style transfer while maintaining the structural integrity of the content image. As illustrated in Fig. 7, the process begins with a given content image  $\mathbf{I}_c$  and a style image  $\mathbf{I}_s$ , along with their corresponding depth maps  $\mathbf{D}_c$  and  $\mathbf{D}_s$ . The style image is first processed by our physics-guided *Waterbody Extractor* [1], which isolates the dominant waterbody characteristics  $\mathbf{B}_s$ . Both  $\mathbf{I}_c$  and  $\mathbf{B}_s$  are then passed

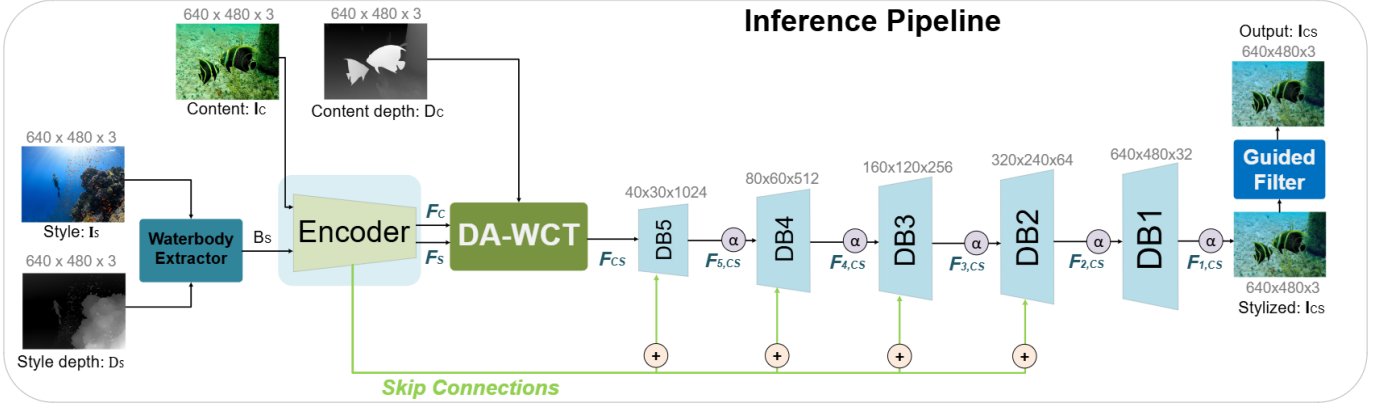


Fig. 7: Inference pipeline of the proposed UStyle model. The content and style images and their corresponding depth maps are first processed through a ResNet-based encoder to extract multi-scale features. These features are processed by our depth-aware whitening and coloring transform (DA-WCT) function for waterbody style alignment, which are then progressively decoded using a multi-stage decoder. Finally, the stylized output is refined with a guided filter to improve visual consistency.

into the *Encoder*, which extracts multi-scale feature representations  $F_c$  and  $F_s$ , respectively. The extracted features are then processed by our *DA-WCT* module, which aligns the feature statistics between content and style domains, producing stylized feature representations  $F_{cs}$ . These transformed features are fed into a multi-stage *Decoder*, each progressively refining the stylized output. Skip connections from the Encoder to the Decoder help retain spatial consistency and fine-grained structural details. At each decoding stage, an adaptive fusion parameter  $\alpha$  controls the style influence level, ensuring smooth content-style integration. Finally, the stylized image  $I_{cs}$  is passed through a *Guided Filter*, which enhances structural coherence and removes unwanted artifacts, yielding the final stylized output  $I_{stylized}$ .

## V. EXPERIMENTAL RESULTS

### A. Baseline Models and Metrics

We use six SOTA models from artistic and photorealistic STx domains as baselines for performance evaluation. Our comparison includes artistic STx methods StyTR-2 [115], ASTMAN [17], MCCNet [16], and IEContraAST [116], alongside the photorealistic method PhotoWCT2 [4]. Additionally, we include AquaFuse [1], a physics-based underwater waterbody style transfer method, to benchmark our approach further. For a fair comparison, all models are fine-tuned on the UF7D dataset; specifically, their pre-trained weights are fine-tuned over 160 K iterations with a batch size of 8 while keeping all other hyperparameters at their recommended settings. For evaluation, we define four cross-domain underwater style transfer test cases: Blue (B)  $\rightarrow$  Green (G), Green (G)  $\rightarrow$  Blue (B), Deep Blue (DB)  $\rightarrow$  Deep Green (DG), and Deep Green (DG)  $\rightarrow$  Deep Blue (DB). Each case consists of 25 content images and 25 style images, generating  $25 \times 25 = 625$  unique test scenes per case, resulting in a total of  $4 \times 625 = 2,500$  test scenes.

**Evaluation Metrics.** We use five standard metrics to evaluate the performance of UStyle and other baseline methods. These complementary metrics assess both the structural preservation and perceptual quality of the stylized images generated by each model. The metrics are:

- **Root Mean Square Error (RMSE)** [117] quantifies pixel-level accuracy between stylized and content images as:  $RMSE = \sqrt{MSE} = \sqrt{\frac{1}{N} \sum_{i=1}^N (x_i - y_i)^2}$ ; where  $x_i$  and  $y_i$  are corresponding pixel values and  $N$  is total number of pixels. The squared difference term amplifies larger errors, making RMSE especially sensitive to outliers and structural distortions.



- **Peak Signal-to-Noise Ratio (PSNR)** [22] measures reconstruction quality as  $\text{PSNR} = 10 \cdot \log_{10} \left( \frac{L^2}{\text{MSE}} \right)$ ; where  $L = 255$  represents the maximum possible pixel value in 8-bit images, and MSE is the mean squared error. PSNR’s logarithmic scale and dependency on  $L$  make it particularly sensitive to illumination changes and global color shifts.
- **Structural Similarity Index (SSIM)** [118] evaluates the geometric consistency of the generated image based on luminance, contrast, and changes in structural information. It is calculated as:

$$\text{SSIM}(x, y) = \frac{(2\mu_x\mu_y + C_1)(2\sigma_{xy} + C_2)}{(\mu_x^2 + \mu_y^2 + C_1)(\sigma_x^2 + \sigma_y^2 + C_2)} \quad (10)$$

where  $\mu$  and  $\sigma$  represent mean and variance respectively, and  $C_1, C_2$  are stability constants. The multiplicative combination of luminance ( $\mu$ ), contrast ( $\sigma$ ), and structure ( $\sigma_{xy}$ ) terms makes SSIM particularly effective for evaluating perceptual image quality.

- **Gradient Magnitude Similarity Deviation (GMSD)** [119] assesses edge preservation by exploiting image gradient information as:  $\text{GMSD} = \sqrt{\frac{1}{N} \sum_{i=1}^N (g_i - \mu_g)^2}$ ; where  $g_i$  represents gradient magnitude similarity at pixel  $i$ , and  $\mu_g$  is the mean. GMSD is particularly effective at detecting structural and textural variations while being relatively insensitive to global illumination changes.
- **Learned Perceptual Image Patch Similarity (LPIPS)** [120] measures perceptual similarity as:

$$\text{LPIPS}(x, y) = \sum_l \frac{1}{H_l W_l} \sum_{h,w} \left\| w_l \odot (\phi_l(x)_{h,w} - \phi_l(y)_{h,w}) \right\|_2^2 \quad (11)$$

Here,  $\phi_l$  represents feature maps from layer  $l$  of a pre-trained network, and  $w_l$  are learned weights that calibrate the importance of different network layers. This metric captures high-level perceptual similarities that often correlate better with human perceptual judgment than traditional metrics.

This combination of metrics enables the evaluation of both low-level image statistics and high-level perceptual qualities. All evaluations are conducted on images normalized to  $640 \times 480$  resolution using their official metric implementations.

## B. Qualitative Results

Figure 8 presents qualitative comparisons across diverse underwater scenes, evaluating four primary waterbody STx cases: B→G, G→B, DB→DG, and DG→DB. Existing artistic STx methods (StyTR-2, ASTMAN, MCCNet, and IEContraAST) struggle to preserve underwater scene realism. Notably, StyTR-2 and ASTMAN introduce noticeable artifacts and texture inconsistencies, distorting natural structures. While MCCNet and IEContraAST improve content preservation, they tend to oversaturate stylized regions, introducing subtle color artifacts. The photorealistic STx method PhotoWCT2 maintains structural integrity in most cases; however, it fails to fully capture deep-water transformations (*e.g.*, DB↔DG). Meanwhile, the physics-based AquaFuse ensures better underwater color consistency, although it requires a carefully curated reference image for optimal performance.

The proposed UStyle method addresses these limitations by incorporating depth awareness into the STx process. Unlike conventional approaches that apply stylization without spatial understanding, UStyle leverages depth supervision to ensure geometric consistency. This advantage is particularly evident in challenging deep-water transitions (DB↔DG), where other methods struggle to balance structural and color fidelity. We hypothesize that UStyle’s superior performance stems from its adaptive multi-stage training and domain-aware waterbody stylization mechanisms (see Sec. V-D for ablation results). Overall, UStyle produces visually coherent, artifact-free stylized outputs that adapt to waterbody style distributions while preserving object geometry and structural integrity.

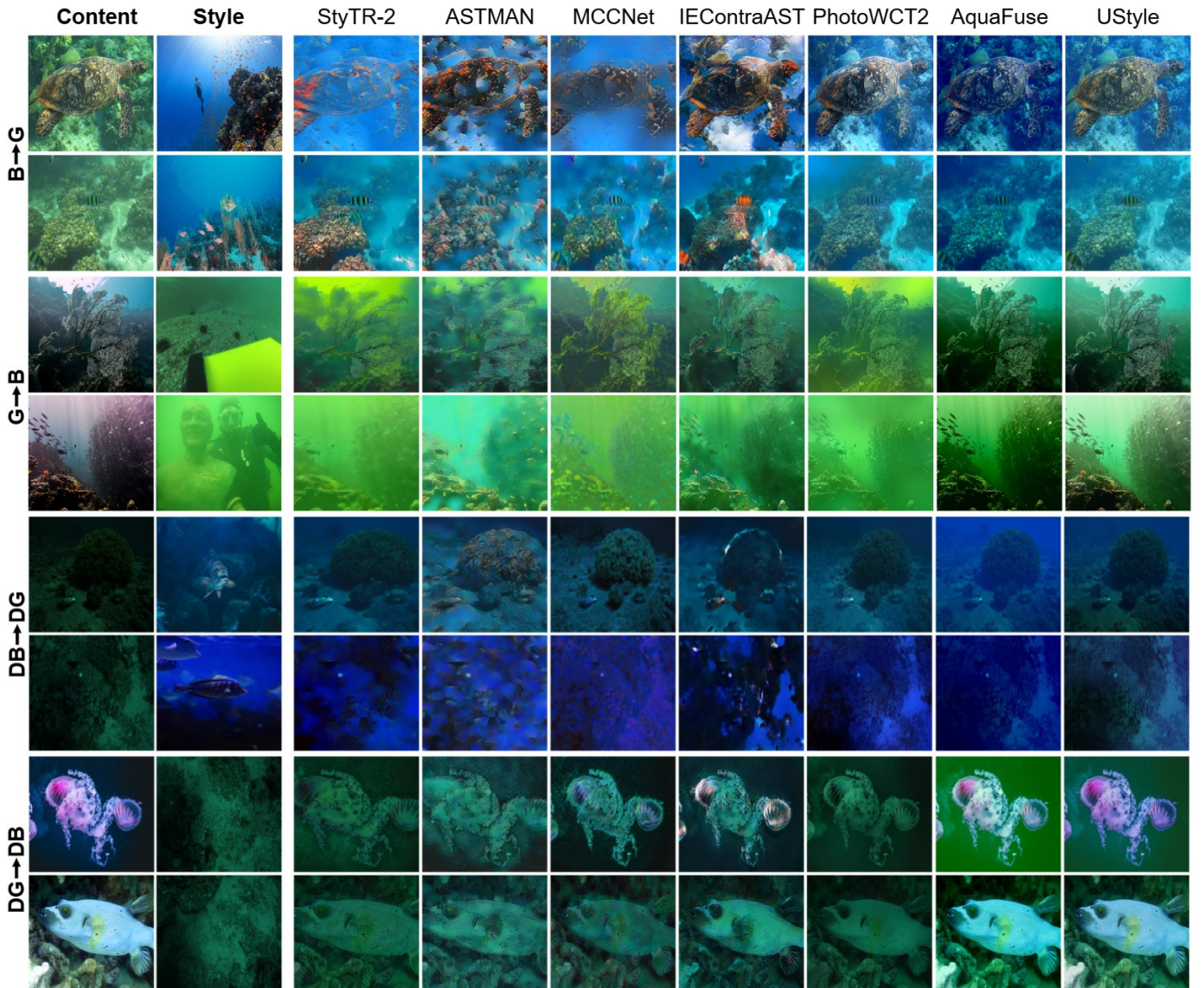


Fig. 8: Qualitative comparison of underwater image style transfer (STx) results across different methods. The first two columns show content and style images, followed by stylized outputs from StyTR-2 [7], ASTMAN [17], MCCNet [6], IEContraAST [5], PhotoWCT2 [4], AquaFuse [1], and UStyle. Each row shows two examples of:  $B \rightarrow G$ ,  $G \rightarrow B$ ,  $DB \rightarrow DG$ , and  $DG \rightarrow DB$  transformations.

### C. Quantitative Results

We conduct a comprehensive quantitative evaluation using five complementary metrics across various underwater STx scenarios from the UF7D test set. As presented in Table I(a), UStyle achieves  $4\times$  to  $6\times$  lower RMSE rates across all scenarios compared to SOTA artistic and photorealistic STx methods. It also consistently outperforms competing approaches in PSNR and SSIM, as shown in Table I(b). The closest competitor, AquaFuse, requires a carefully selected reference image and prior information such as incident angle and attenuation characteristics. In contrast, UStyle achieves improvements of 15% (RMSE), 5.29% (PSNR), and 5.71% (SSIM) over AquaFuse while operating without any reference or prior knowledge — demonstrating its robustness and accuracy for waterbody STx.

We further provide a quantitative comparison of perceptual metrics, including GMSD and LPIPS, as

TABLE I: Quantitative comparison of averaged RMSE ( $\downarrow$ ), PSNR ( $\uparrow$ ), and SSIM ( $\uparrow$ ) across different underwater STx methods are conducted on 2,500 test samples in UF7D. The best score is highlighted in **bold blue**, while the second-best is shown in **blue**.

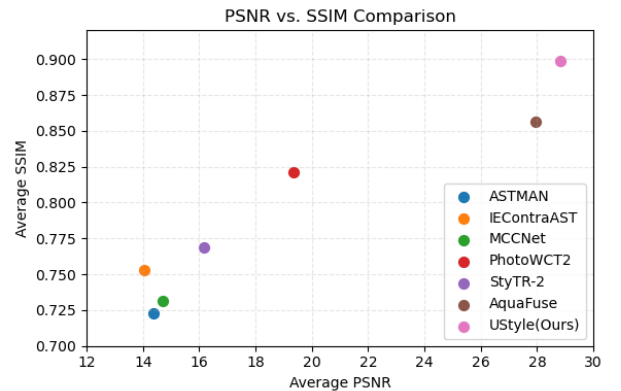
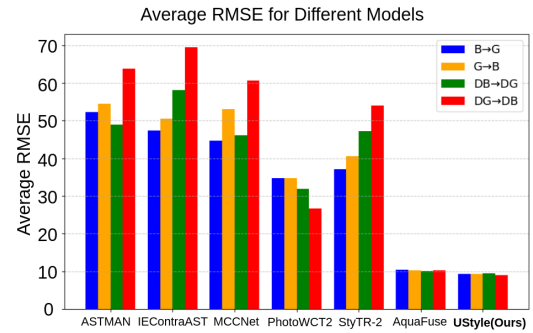
| (a) RMSE $\downarrow$ | B $\rightarrow$ G | G $\rightarrow$ B | DB $\rightarrow$ DG | DG $\rightarrow$ DB |
|-----------------------|-------------------|-------------------|---------------------|---------------------|
| ASTMAN [17]           | 52.29             | 54.53             | 48.91               | 63.74               |
| IEContraAST [116]     | 47.32             | 50.54             | 58.17               | 69.49               |
| MCCNet [16]           | 44.64             | 53.12             | 46.04               | 60.71               |
| PhotoWCT2 [4]         | 34.68             | 34.80             | 31.89               | 26.66               |
| StyTR-2 [115]         | 37.08             | 40.61             | 47.18               | 54.01               |
| AquaFuse [1]          | <b>10.45</b>      | <b>10.19</b>      | <b>10.15</b>        | <b>10.24</b>        |
| UStyle                | <b>9.39</b>       | <b>9.35</b>       | <b>9.50</b>         | <b>8.96</b>         |

| (b) PSNR $\uparrow$ | B $\rightarrow$ G | G $\rightarrow$ B | DB $\rightarrow$ DG | DG $\rightarrow$ DB |
|---------------------|-------------------|-------------------|---------------------|---------------------|
| ASTMAN [17]         | 14.95             | 14.37             | 14.99               | 13.16               |
| IEContraAST [116]   | 15.90             | 14.40             | 13.82               | 12.10               |
| MCCNet [16]         | 15.81             | 14.01             | 15.63               | 13.35               |
| PhotoWCT2 [4]       | 19.75             | 18.70             | 18.95               | 20.05               |
| StyTR-2 [115]       | 17.86             | 16.67             | 15.59               | 14.58               |
| AquaFuse [1]        | <b>27.77</b>      | <b>28.00</b>      | <b>28.03</b>        | <b>27.94</b>        |
| UStyle              | <b>28.73</b>      | <b>28.72</b>      | <b>28.64</b>        | <b>29.14</b>        |

| (c) SSIM $\uparrow$ | B $\rightarrow$ G | G $\rightarrow$ B | DB $\rightarrow$ DG | DG $\rightarrow$ DB |
|---------------------|-------------------|-------------------|---------------------|---------------------|
| ASTMAN [17]         | 0.8026            | 0.6334            | 0.8150              | 0.6397              |
| IEContraAST [116]   | 0.7641            | 0.6304            | 0.7887              | 0.6033              |
| MCCNet [16]         | 0.8095            | 0.6302            | 0.8290              | 0.6570              |
| PhotoWCT2 [4]       | 0.8675            | 0.7819            | <b>0.8324</b>       | 0.8030              |
| StyTR-2 [115]       | 0.8494            | 0.6937            | 0.8199              | 0.7125              |
| AquaFuse [1]        | <b>0.9337</b>     | <b>0.8708</b>     | 0.7394              | <b>0.8812</b>       |
| UStyle              | <b>0.9613</b>     | <b>0.8818</b>     | <b>0.8389</b>       | <b>0.9126</b>       |



(d) Average RMSE scores are shown on (top barchart) and the PSNR–SSIM scores are visualized in a 2D grid (bottom); evident from these results, UStyle achieves better overall performance than existing STx methods.

summarized in Table II. The results demonstrate that UStyle achieves superior preservation of both low-level image statistics and high-level perceptual fidelity. Notably, it attains the lowest LPIPS scores, with values of 0.1926 (B $\rightarrow$ G), 0.2235 (G $\rightarrow$ B), 0.1342 (DB $\rightarrow$ DG), and 0.1373 (DG $\rightarrow$ DB). In comparison, PhotoWCT2 exhibits an LPIPS range of 0.1676–0.2618, while artistic stylization methods such as ASTMAN and MCCNet perform less effectively, exceeding 0.3 in most transformations. Furthermore, UStyle consistently achieves the lowest GMSD scores across all test cases. The accompanying heatmap visualizations in Table II(c) further illustrate UStyle’s superior performance for combined deviations of each model based on GMSD and LPIPS. These findings align with our qualitative analyses, reinforcing that UStyle enables robust and perceptually accurate waterbody style transfer while preserving the structural integrity of the scene.

#### D. Ablation Studies

We conduct ablation experiments to evaluate the key components of UStyle: (i) the impact of depth supervision in the stylization process and (ii) the contribution of various loss components to STx performance. To assess the role of depth supervision, we compare stylized results with and without depth guidance. As shown in Fig. 9, DA-WCT improves structural retention and color adaptation in complex

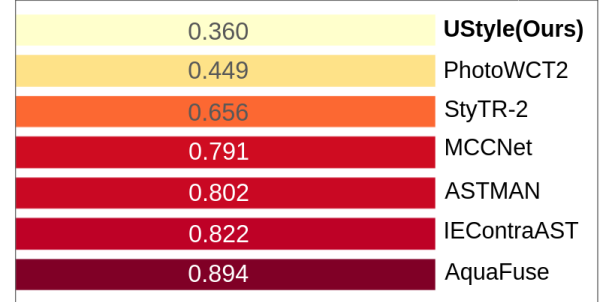
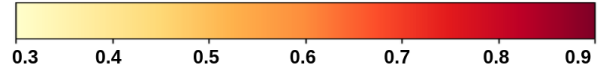


TABLE II: Quantitative comparison of averaged GMSD ( $\downarrow$ ) and LPIPS ( $\downarrow$ ) across different underwater STx methods, conducted on 2,500 test samples in UF7D. The best score is highlighted in **bold blue**, while the second-best is shown in **blue**.

| (a) GMSD $\downarrow$ | B $\rightarrow$ G | G $\rightarrow$ B | DB $\rightarrow$ DG | DG $\rightarrow$ DB |
|-----------------------|-------------------|-------------------|---------------------|---------------------|
| ASTMAN [17]           | 0.0693            | 0.0318            | 0.0508              | <b>0.0179</b>       |
| IEContraAST [116]     | 0.0694            | 0.0300            | 0.0556              | <b>0.0187</b>       |
| MCCNet [16]           | 0.0262            | <b>0.0107</b>     | 0.0386              | 0.0386              |
| PhotoWCT2 [4]         | 0.0622            | 0.0725            | 0.0762              | 0.0386              |
| StyTR-2 [115]         | 0.0551            | <b>0.0287</b>     | 0.0380              | 0.0187              |
| AquaFuse [1]          | <b>0.0252</b>     | 0.0631            | <b>0.0201</b>       | 0.0471              |
| UStyle                | <b>0.0227</b>     | 0.0564            | <b>0.0200</b>       | 0.0431              |

| (b) LPIPS $\downarrow$ | B $\rightarrow$ G | G $\rightarrow$ B | DB $\rightarrow$ DG | DG $\rightarrow$ DB |
|------------------------|-------------------|-------------------|---------------------|---------------------|
| ASTMAN [17]            | 0.2992            | 0.4849            | 0.3769              | 0.4091              |
| IEContraAST [116]      | 0.2762            | 0.4835            | 0.3896              | 0.4518              |
| MCCNet [16]            | 0.2838            | 0.4976            | 0.3677              | 0.3989              |
| PhotoWCT2 [4]          | <b>0.1676</b>     | <b>0.2618</b>     | <b>0.2409</b>       | <b>0.1755</b>       |
| StyTR-2 [115]          | 0.2372            | 0.3612            | 0.3624              | 0.3261              |
| AquaFuse [1]           | 0.4274            | 0.3902            | 0.5597              | 0.3789              |
| UStyle                 | <b>0.1926</b>     | <b>0.2235</b>     | <b>0.1342</b>       | <b>0.1373</b>       |



(c) A heatmap illustrating the combined deviation, which represents the overall distortion by each model, computed by GMSD and LPIPS scores. Here, lower values indicate better overall performance; UStyle achieves the lowest score, 19.8% lower than the closest competitor.

underwater scenes. Without depth supervision, stylized images exhibit color distortions and detail loss, whereas DA-WCT preserves content integrity throughout the STx process.

Additionally, we investigate the contribution of different loss components by evaluating three configurations of our model: (1) UStyle without clip loss (w/o CLIP), (2) UStyle without additional regularization losses,  $L3 = \mathcal{L}_{sim} + \mathcal{L}_{color} + \mathcal{L}_{fft}$  (w/o  $L3$ ), and (3) UStyle with all loss components. Table III presents the quantitative comparison across PSNR, SSIM, and RMSE for four underwater style transfer scenarios. The results show that the full UStyle model consistently performs better, demonstrating the effectiveness of depth supervision and loss regularization. From a quantitative perspective, depth supervision leads to a substantial improvement in all three metrics. The inclusion of additional losses further refines the model’s ability to balance structural preservation and perceptual realism. The full UStyle model achieves the highest PSNR and SSIM values while maintaining the lowest RMSE across all scenarios.

To further examine the impact of DA-WCT stylization, we employ Grad-CAM [121] visualizations to highlight the regions of interest in our model’s decision-making process. As illustrated in Fig. 10, depth supervision enables UStyle to focus more effectively on salient structures, ensuring spatially coherent style adaptation. The middle row displays activation maps generated with depth guidance, where attention is evenly distributed across foreground and background elements, enhancing structure retention. In contrast, the bottom row—corresponding to the model without depth supervision—reveals inconsistent attention patterns, leading to fine-detail loss and exaggerated distortions. Notably, DA-WCT ensures that complex structures, such as marine organisms and underwater artifacts, are better preserved by aligning style fusion with content depth information. These visualizations further validate the importance of incorporating depth guidance, reinforcing its role in improving geometric consistency and reducing artifacts in waterbody STx.

These findings confirm that **depth supervision** is essential for maintaining spatial coherence and content preservation in underwater STx. Furthermore, integrating additional **regularization losses** significantly enhances perceptual quality, reducing distortions and improving color adaptation.





Fig. 9: A few ablation results illustrating the impact of depth-guidance in the stylization process. With the proposed DA-WCT blending, stylized outputs exhibit consistent blending, both on foreground objects and background waterbody regions. In contrast, we observe a global averaging effect while using only WCT and over-saturated pixels for deep-water (DB/DG) styles.

TABLE III: For ablation study, we compare the performance of three variants: UStyle without clip loss (w/o CLIP), UStyle without additional regularization losses  $L3$  (w/o  $L3$ ), and UStyle with all loss components. Each of these variants is evaluated with WCT/DA-WCT on PSNR ( $\uparrow$ ), SSIM ( $\uparrow$ ), and RMSE ( $\downarrow$ ) metrics.

| Data   |                       | B $\rightarrow$ G |        | G $\rightarrow$ B |        | DB $\rightarrow$ G |        | DG $\rightarrow$ B |        |
|--------|-----------------------|-------------------|--------|-------------------|--------|--------------------|--------|--------------------|--------|
| Metric | Model                 | WCT               | DA-WCT | WCT               | DA-WCT | WCT                | DA-WCT | WCT                | DA-WCT |
| PSNR   | 1: UStyle (w/o CLIP)  | 28.03             | 28.69  | 28.24             | 28.69  | 27.85              | 28.00  | 28.39              | 29.09  |
|        | 2: UStyle (w/o $L3$ ) | 27.96             | 28.36  | 28.21             | 28.64  | 27.84              | 27.91  | 28.43              | 28.97  |
|        | 3: UStyle (Full)      | 28.09             | 28.73  | 28.24             | 28.72  | 27.91              | 28.64  | 28.43              | 29.14  |
| SSIM   | 1: UStyle (w/o CLIP)  | 0.9319            | 0.9549 | 0.8090            | 0.8758 | 0.6365             | 0.8046 | 0.8421             | 0.9102 |
|        | 2: UStyle (w/o $L3$ ) | 0.9337            | 0.9590 | 0.8004            | 0.8675 | 0.6087             | 0.7780 | 0.8388             | 0.9069 |
|        | 3: UStyle (Full)      | 0.9349            | 0.9613 | 0.8260            | 0.8818 | 0.6727             | 0.8389 | 0.8506             | 0.9126 |
| RMSE   | 1: UStyle (w/o CLIP)  | 10.15             | 9.43   | 9.90              | 9.40   | 10.37              | 10.19  | 9.75               | 9.01   |
|        | 2: UStyle (w/o $L3$ ) | 10.23             | 9.77   | 9.93              | 9.45   | 10.38              | 10.28  | 9.70               | 9.15   |
|        | 3: UStyle (Full)      | 10.08             | 9.39   | 9.89              | 9.35   | 10.31              | 9.50   | 9.70               | 8.96   |

### E. Analysis of Results

Our comprehensive evaluation indicates that UStyle offers superior quantitative performance and stable training behavior. We observed that the progressive blockwise training strategy [20] enabled the network to gradually refine its multi-scale feature representations without significant oscillations in loss values, consistently improving structural fidelity and perceptual quality. For instance, as shown in Table I, UStyle achieves an average RMSE of 8.96, which is approximately 10-16% lower than the values reported by physics-based approaches that range from 10.15 to 10.45, respectively, indicating a notable enhancement in

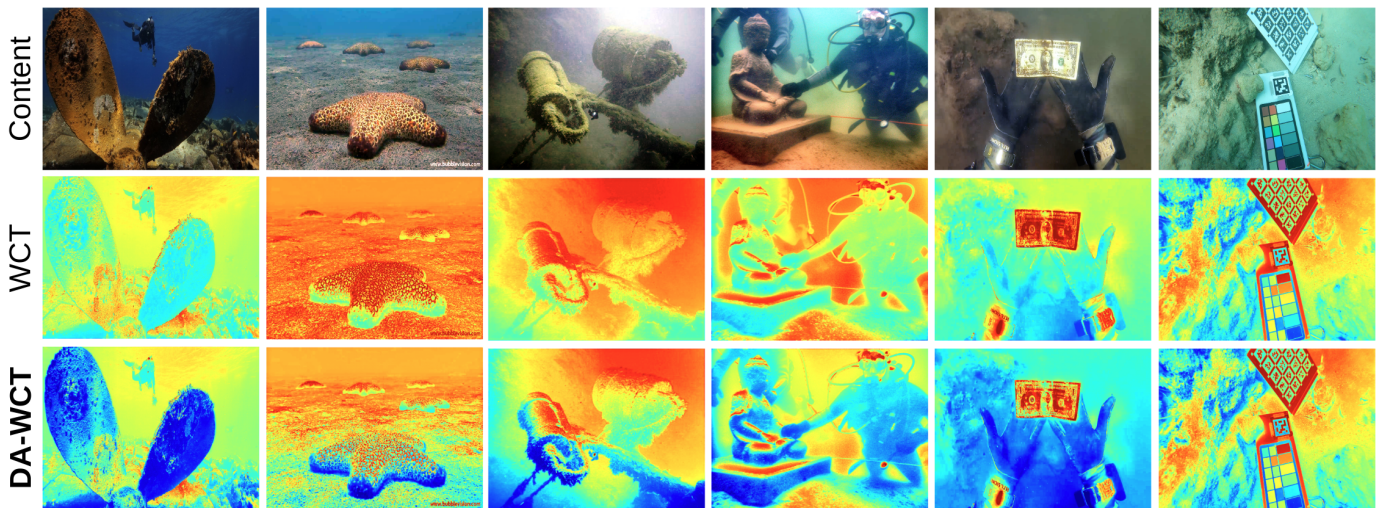


Fig. 10: Grad-CAM heatmap visualizing the effect of depth-aware style fusion in UStyle. Our DA-WCT enhances attention to structural details, ensuring a more spatially coherent style adaptation (third row). In comparison, without depth supervision, attention is unevenly distributed, leading to potential distortions and loss of fine details in complex underwater scenes (second row).

reconstruction accuracy. In addition, the perceptual metrics reveal that UStyle attains LPIPS scores as low as 0.1373 for the DG→DB transformation and GMSD values around 0.02, underscoring its effectiveness in preserving edge details and minimizing perceptual distortions. Ablation studies indicate that incorporating depth-aware mechanisms improves SSIM by about 4.5% and reduces RMSE by approximately 10.3%.

Complementary to these numerical results, the Grad-CAM [121] visualizations in Figure 10 illustrate that depth guidance enables more uniform and focused attention across critical image regions, ensuring spatial coherence. These findings suggest that the DA-WCT module guides the network to focus on relevant salient structural cues while mitigating artifacts. Moreover, the training process revealed that UStyle consistently converges across diverse underwater conditions without manual parameter tuning, unlike physics-based models, which are sensitive to reference image quality and scene priors. Overall, UStyle’s design choices yield a robust and efficient framework for underwater STx, and these insights may guide future research in developing even more adaptive and efficient solutions.

Furthermore, during inference using UStyle and the baseline models, we noticed that models without depth guidance, mainly when applied to deep-water style transitions, frequently produced over-saturated outputs with a global averaging effect [122]; this resulted in increased RMSE values by approximately 10% to 12% and LPIPS scores that were consistently higher. In contrast, UStyle maintained stable convergence and demonstrated a more consistent loss decay pattern with a reduction in loss variance of about 15%. Furthermore, the inclusion of the CLIP loss [25] in UStyle contributed to a smoother convergence trajectory by aligning semantic features; removal of this component led to slight degradations in SSIM (a reduction of roughly 0.002 on average) and a marginal increase in RMSE, highlighting the importance of semantic consistency in waterbody STx learning.

Additional observations from our experiments reveal that UStyle’s adaptive multi-stage training strategy [20] resulted in convergence speeds approximately 20% faster than several baseline models. The fine-tuning process on underwater-specific data proved crucial for the network to adapt to domain-specific distortions, yielding significant improvements in performance metrics across diverse underwater scenarios. This indicates that carefully designed loss functions, particularly those focusing on structural similarity [22], color consistency [21], and frequency-domain fidelity [23], are essential for achieving



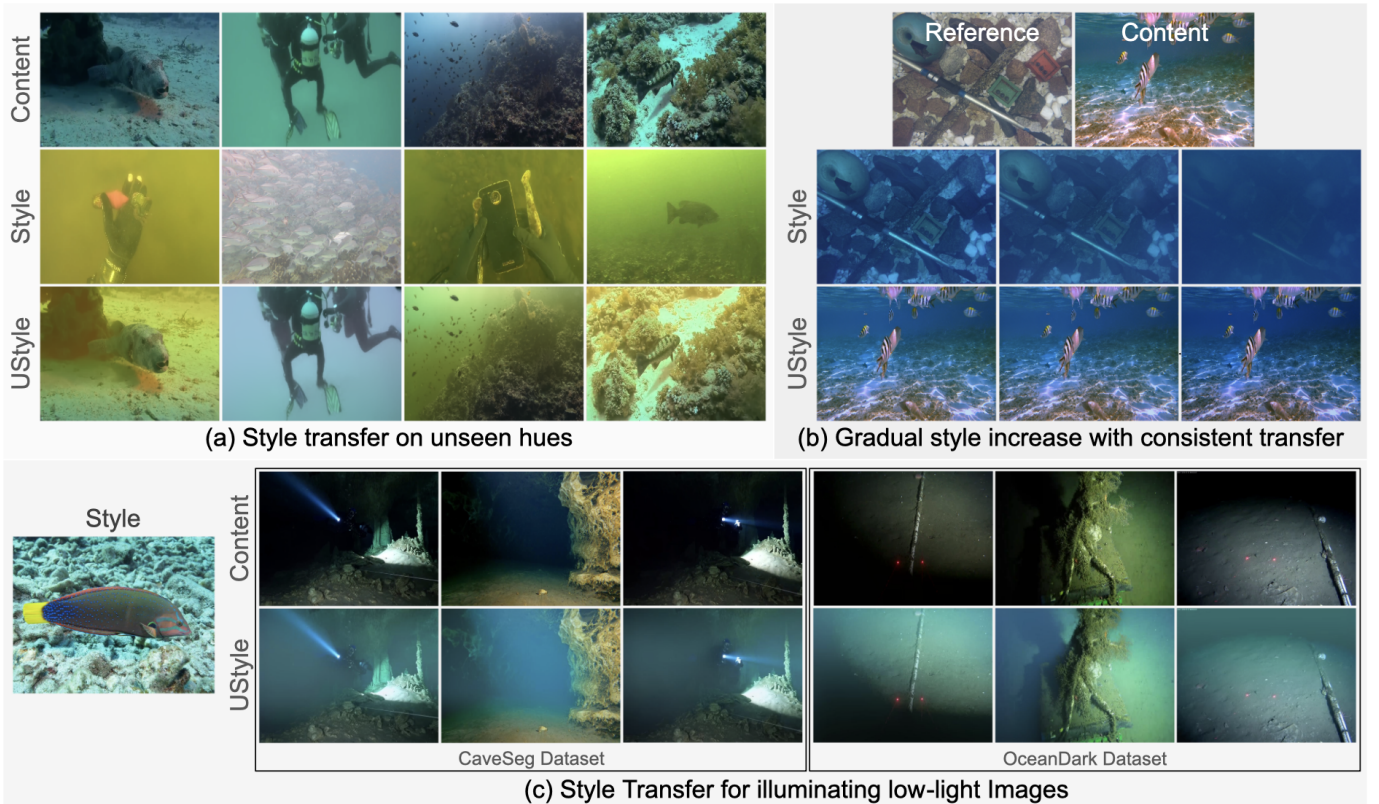


Fig. 11: Evaluation of UStyle’s generalization capability under three unseen scenarios: (a) Style transfer on previously unseen color hues (yellow and grey) from UIEB [123], (b) Consistent interpolation across progressively intensified waterbody styles from the TURBID [124] dataset, (c) Illumination of low-light underwater scenes from CaveSeg [125] and OceanDark [126] datasets using a well-lit image as style.

high-quality results in complex underwater environments.

During waterbody fusion, we observed that the depth maps’ quality and depth thresholding precision influenced the stylization process. Variations in depth maps lead to noticeable differences in the retention of fine details, especially in regions with subtle gradient changes. Our future research will emphasize robust depth extraction methods and consider dynamic adjustment of depth-based parameters to enhance performance further. Additionally, the success of UStyle in handling diverse underwater conditions without reliance on manually curated reference images with explicit scene priors suggests that its framework may be extended to other domains where scene priors are challenging to obtain.

## VI. GENERALIZATION PERFORMANCE

### A. Unseen Style Transfer

The generalization ability of UStyle is validated through three distinct scenarios as shown in Figure 11, using the model trained on the UF7D dataset without any additional fine-tuning. First, in Figure 11 (a), We used UIEB [123], which feature unseen waterbody hues such as grey and yellow, distinct from the predominantly blue and green hues seen during training. UStyle demonstrated its ability to transfer these unseen hues onto the content images, highlighting its strong generalization capability and robust style representation learned from the UF7D dataset. Next, we examine gradual style intensification using the TURBID [124] dataset in Figure 11 (b). This dataset provides images that are originally clear, along with corresponding versions exhibiting progressively increasing levels of turbidity (light to dark blue tone).

Using these as style references, we observe that UStyle performs smooth and consistent style transfer across all levels of distortion, indicating its ability to interpolate within a continuous style manifold.

Figure 11 emphasized the practical significance of UStyle by evaluating style transfer in low-light underwater conditions using images from the CaveSeg [125] and OceanDark [126] datasets. We applied a well-lit, high-quality style image to dimly illuminated underwater scenes. UStyle effectively transferred the brighter illumination conditions from the reference style image, enhancing visibility and clarifying structural details. This capability demonstrates a meaningful practical application, showcasing how UStyle can be effectively utilized for other underwater imaging tasks.

### B. Computational Analyses

As shown in Table IV, UStyle maintains a stable inference rate across multiple resolutions. Evaluated on a single NVIDIA A100 GPU, UStyle processes a  $256 \times 256$  image in approximately 518ms and a full HD  $1920 \times 1080$  image in about 741ms. While transformer-based methods such as StyTr2 [7] and IEContraAST [5] struggle with high-resolution images due to high memory consumption, UStyle consistently operates across all resolutions, demonstrating scalability. Although MCCNet [115] and ASTMAN [17] achieve faster processing times at low resolutions, their performance is not comparable to UStyle. Moreover, due to memory constraints, StyTr2 [7], ASTMAN [17], and IEContraAST [5] fail to process images at resolutions beyond  $1280 \times 720$  as well. While UStyle is not intended for real-time applications, rather a high-performance data augmentation and stylization tool, it still provides competitive processing speeds, especially at high input resolutions.

TABLE IV: Inference speed based on image processing time per image (msec  $\downarrow$ ) across different image resolutions for six data-driven SOTA methods are shown. Evaluations are performed on a single NVidia A100 GPU with 16 GB RAM; ‘ $\times$ ’ indicates the out-of-memory (OOM) cases.

| Resolution      | $256 \times 256$ | $512 \times 512$ | $640 \times 480$ | $1024 \times 1024$ | $1280 \times 720$ | $1920 \times 1080$ | $3840 \times 2160$ |
|-----------------|------------------|------------------|------------------|--------------------|-------------------|--------------------|--------------------|
| ASTMAN [17]     | 180              | 190.8            | 222.7            | 250.6              | 227.8             | 274.0              | $\times$           |
| IEContraAST [5] | 1219.5           | 2127.7           | 2272.7           | 2702.7             | 3125.0            | 4761.9             | $\times$           |
| MCCNet [6]      | 170.9            | 209.2            | 229.4            | 354.6              | 371.7             | 549.5              | 1886.8             |
| StyTr2 [7]      | 136.2            | 274.7            | 285.7            | 1639.3             | 2040.8            | $\times$           | $\times$           |
| PhotoWCT2 [4]   | 323.6            | 340.1            | 344.8            | 390.6              | 374.5             | 467.3              | 885.0              |
| <b>UStyle</b>   | 518.1            | 621.1            | 641.0            | 645.2              | 645.2             | 740.7              | 1087.0             |

### C. Benefits Over AquaFuse

As we discussed earlier in Sec. IV-C, we use a physics-guided waterbody synthesis module of AquaFuse [1] to extract the waterbody characteristics from the style image. Note that AquaFuse synthesizes the content image by incorporating a reference scene’s waterbody through a physics-guided approximation approach. However, this method relies on a noise-free reference image and prior scene information, including depth, incident angle, and attenuation parameters. As illustrated in Figure 12, AquaFuse is highly sensitive to input parameters such as incident angles and tuned attenuation coefficients, limiting its generalizability across diverse underwater conditions. Its performance is strongly influenced by the choice of reference image and variations in incident angles. In contrast, UStyle, a learning-based STx framework, adapts robustly to varying aquatic environments without requiring manually tuned priors. To facilitate this adaptability, large-scale datasets such as USOD10K and UF7D provide a diverse collection of waterbody styles, enabling more generalized STx learning, as demonstrated in our experimental analyses.



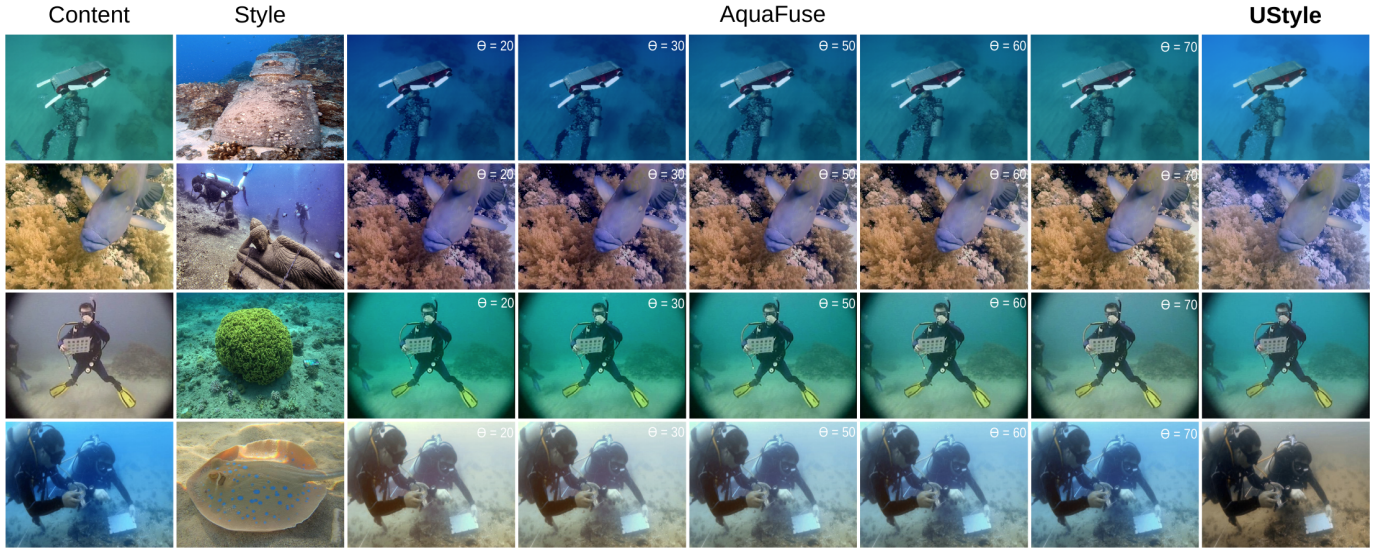


Fig. 12: Comparison between AquaFuse and UStyle across different underwater scenes. The first three rows show that AquaFuse outputs are highly sensitive to the choice of incident angle; the last row further shows that selecting a wrong reference image can significantly impact its waterbody fusion process. UStyle is invariant to these dependencies, offering consistent waterbody STx performance.

#### D. Limitations and Future Directions

Although UStyle demonstrates robust performance and achieves SOTA results, several aspects of the framework warrant further refinement. In particular, enhancements in depth estimation accuracy, training efficiency, adaptive handling of specific waterbody styles, and performance under extreme turbidity conditions remain as challenging cases; more details are listed below.

- **Dependency on depth estimation:** UStyle’s performance, as dependent on the DA-WCT module, depends on the quality of depth maps, which can be unreliable in noisy sensing conditions and severely attenuated scenes. Future work could incorporate self-supervised depth estimation methods to enhance robustness and reduce dependency on precomputed scene depth estimation.
- **Training and inference efficiency:** Although the progressive blockwise training strategy enhances convergence stability and multi-scale feature learning, it increases training time compared to single-stage models. Future work could explore the design of lightweight architectures or leverage knowledge distillation techniques [127] to improve efficiency without sacrificing the generalization performance.
- **Extremely turbid or rare waterbody styles:** The compounded effects of scattering and absorption can significantly impair style transfer quality for severely turbid scenes [128]. Future work will explore integrating polarization-based enhancement techniques [129] and multi-spectral image enhancement methods [130] to improve UStyle’s robustness in challenging underwater environments. We will also explore adaptive blending mechanisms [131] to better accommodate rare/unseen waterbody styles.

Despite these challenges, UStyle significantly advances underwater STx literature for data-driven waterbody fusion. Future research will optimize its efficiency, extend it to real-time video applications, and improve robustness in complex underwater scenarios.

## VII. CONCLUSION

In this work, we presented UStyle, the first data-driven framework for underwater waterbody style transfer that robustly fuses waterbody characteristics without relying on manually curated reference

images with explicit scene priors. Leveraging a ResNet-based encoder-decoder architecture, a progressive blockwise training strategy, and a novel depth-aware whitening and coloring transform (DA-WCT), UStyle effectively preserves structural integrity while achieving perceptually compelling stylization. Extensive quantitative and qualitative evaluations demonstrate that UStyle outperforms SOTA artistic, photorealistic, and physics-based methods, achieving improvements of up to 16% in RMSE, reaching PSNR values of 29.14 dB, SSIM values as high as 0.9613, and attaining LPIPS scores as low as 0.1373. Ablation studies further confirm that integrating depth supervision and additional regularization losses is critical for enhancing geometric consistency and minimizing perceptual distortions. Moreover, computational analyses reveal that UStyle maintains stable inference rates across various resolutions, showcasing its scalability for high-resolution underwater imaging applications. Although challenges remain in handling extreme turbidity and further optimizing training efficiency, our findings underscore the potential of UStyle as a robust tool for underwater imaging, data augmentation, and vision tasks. Future work will incorporate depth estimation, explore lightweight architectures for real-time applications, and extend the framework to handle more complex underwater STx scenarios in real-time.

#### ACKNOWLEDGMENTS

This work is supported in part by the National Science Foundation (NSF) grant #2330416 and the University of Florida (UF) research grant #132763.

#### REFERENCES

- [1] M. Siddique, J. Wu, I. Rekleitis, and M. J. Islam, "AquaFuse: Waterbody Fusion for Physics Guided View Synthesis of Underwater Scenes," *IEEE Robotics and Automation Letters (RA-L)*, 2025.
- [2] Y. Chen, Q. Yuan, Z. Li, Y. Liu, W. Wang, C. Xie, X. Wen, and Q. Yu, "Upst-nerf: Universal photorealistic style transfer of neural radiance fields for 3d scene," *IEEE Transactions on Visualization and Computer Graphics*, 2024.
- [3] Y. Zheng, J. Jiao, F. Ye, Y. Zhou, and W. Li, "Fast style transfer for ethnic patterns innovation," *Expert Systems with Applications*, vol. 249, p. 123627, 2024.
- [4] T.-Y. Chiu and D. Gurari, "Photowct2: Compact autoencoder for photorealistic style transfer resulting from blockwise training and skip connections of high-frequency residuals," in *Proceedings of the IEEE Winter Conference on Applications of Computer Vision (WACV)*, 2022, pp. 2867–2877.
- [5] H. Chen, Z. Wang, H. Zhang, Z. Zuo, A. Li, W. Xing, D. Lu *et al.*, "Artistic style transfer with internal-external learning and contrastive learning," *Advances in Neural Information Processing Systems*, vol. 34, pp. 26 561–26 573, 2021.
- [6] Y. Deng, F. Tang, W. Dong, H. Huang, C. Ma, and C. Xu, "Arbitrary video style transfer via multi-channel correlation," in *Proceedings of the AAAI Conference on Artificial Intelligence*, vol. 35, no. 2, 2021, pp. 1210–1217.
- [7] Y. Deng, F. Tang, W. Dong, C. Ma, X. Pan, L. Wang, and C. Xu, "Stytr2: Image style transfer with transformers," in *Proceedings of the IEEE/CVF conference on computer vision and pattern recognition*, 2022, pp. 11 326–11 336.
- [8] D. Akkaynak and T. Treibitz, "A Revised Underwater Image Formation Model," in *IEEE Conference on Computer Vision and Pattern Recognition (CVPR)*, 2018, pp. 6723–6732.
- [9] G. Kwon and J. C. Ye, "Clipstyler: Image style transfer with a single text condition," in *Proceedings of the IEEE/CVF conference on computer vision and pattern recognition*, 2022, pp. 18 062–18 071.
- [10] S. Yang, H. Hwang, and J. C. Ye, "Zero-shot contrastive loss for text-guided diffusion image style transfer," in *Proceedings of the IEEE/CVF International Conference on Computer Vision*, 2023, pp. 22 873–22 882.
- [11] C. Li, C. Guo, W. Ren, R. Cong, J. Hou, S. Kwong, and D. Tao, "An underwater image enhancement benchmark dataset and beyond," *IEEE Transactions on Image Processing*, vol. 29, pp. 4376–4389, 2019.
- [12] D. Akkaynak and T. Treibitz, "Sea-thru: A method for removing water from underwater images," in *Proceedings of the IEEE/CVF conference on computer vision and pattern recognition*, 2019, pp. 1682–1691.
- [13] L. Peng, C. Zhu, and L. Bian, "U-shape transformer for underwater image enhancement," *IEEE Transactions on Image Processing*, vol. 32, pp. 3066–3079, 2023.
- [14] M. J. Islam, S. S. Enan, P. Luo, and J. Sattar, "Underwater image super-resolution using deep residual multipliers," in *2020 IEEE International Conference on Robotics and Automation (ICRA)*. IEEE, 2020, pp. 900–906.
- [15] M. J. Islam, Y. Xia, and J. Sattar, "Fast Underwater Image Enhancement for Improved Visual Perception," *IEEE Robotics and Automation Letters (RA-L)*, vol. 5, no. 2, pp. 3227–3234, 2020.
- [16] Y. Wang, S. Yang, P. Wu, Y. Chen, W. An, X. Wang, and D. Xu, "Arbitrary video style transfer via multi-channel correlation," in *Proceedings of the IEEE/CVF Conference on Computer Vision and Pattern Recognition (CVPR)*, 2020, pp. 8178–8187.

- [17] Y. Deng, F. Tang, W. Dong, C. Ma, and C. Xu, "Arbitrary style transfer via multi-adaptation network," in *Proceedings of the 28th ACM International Conference on Multimedia*, 2020, pp. 2594–2602.
- [18] B. Koonce and B. Koonce, "Resnet 50," *Convolutional neural networks with swift for tensorflow: image recognition and dataset categorization*, pp. 63–72, 2021.
- [19] Y. Seo and K.-s. Shin, "Hierarchical convolutional neural networks for fashion image classification," *Expert systems with applications*, vol. 116, pp. 328–339, 2019.
- [20] H. Wang, H. Zhao, X. Li, and X. Tan, "Progressive blockwise knowledge distillation for neural network acceleration," in *IJCAI*, 2018, pp. 2769–2775.
- [21] L. Dong, W. Zhang, and W. Xu, "Underwater image enhancement via integrated rgb and lab color models," *Signal Processing: Image Communication*, vol. 104, p. 116684, 2022.
- [22] A. Hore and D. Ziou, "Image quality metrics: Psnr vs. ssim," *2010 20th International Conference on Pattern Recognition*, pp. 2366–2369, 2010.
- [23] E. O. Brigham, *The fast Fourier transform and its applications*. Prentice-Hall, Inc., 1988.
- [24] K. Simonyan and A. Zisserman, "Very deep convolutional networks for large-scale image recognition," *arXiv preprint arXiv:1409.1556*, 2014.
- [25] A. Radford, J. W. Kim, C. Hallacy, A. Ramesh, G. Goh, S. Agarwal, G. Sastry, A. Askell, P. Mishkin, J. Clark *et al.*, "Learning transferable visual models from natural language supervision," in *International conference on machine learning*. PmLR, 2021, pp. 8748–8763.
- [26] L. A. Gatys, A. S. Ecker, and M. Bethge, "A neural algorithm of artistic style," *arXiv preprint arXiv:1508.06576*, 2015.
- [27] R. Wang *et al.*, "Research on image generation and style transfer algorithm based on deep learning," *Open Journal of Applied Sciences*, vol. 9, no. 08, p. 661, 2019.
- [28] Y. Zhang, Y. Zhang, and W. Cai, "A unified framework for generalizable style transfer: Style and content separation," *IEEE Transactions on Image Processing*, vol. 29, pp. 4085–4098, 2020.
- [29] F. Luan, S. Paris, E. Shechtman, and K. Bala, "Deep photo style transfer," in *Proceedings of the IEEE conference on computer vision and pattern recognition*, 2017, pp. 4990–4998.
- [30] S. S. Kim, N. Kolkin, J. Salavon, and G. Shakhnarovich, "Deformable style transfer," in *Computer Vision—ECCV 2020: 16th European Conference, Glasgow, UK, August 23–28, 2020, Proceedings, Part XXVI 16*. Springer, 2020, pp. 246–261.
- [31] Y. Lyu, Y. Jiang, B. Peng, and J. Dong, "Infostyler: Disentanglement information bottleneck for artistic style transfer," *IEEE Transactions on Circuits and Systems for Video Technology*, vol. 34, no. 4, pp. 2070–2082, 2023.
- [32] Y. Zhang, N. Huang, F. Tang, H. Huang, C. Ma, W. Dong, and C. Xu, "Inversion-based style transfer with diffusion models," in *Proceedings of the IEEE/CVF conference on computer vision and pattern recognition*, 2023, pp. 10 146–10 156.
- [33] Z. Wang, L. Zhao, and W. Xing, "Stylediffusion: Controllable disentangled style transfer via diffusion models," in *Proceedings of the IEEE/CVF International Conference on Computer Vision*, 2023, pp. 7677–7689.
- [34] J. Chung, S. Hyun, and J.-P. Heo, "Style injection in diffusion: A training-free approach for adapting large-scale diffusion models for style transfer," in *Proceedings of the IEEE/CVF Conference on Computer Vision and Pattern Recognition*, 2024, pp. 8795–8805.
- [35] S. Li, "Diffstyler: Diffusion-based localized image style transfer," *arXiv preprint arXiv:2403.18461*, 2024.
- [36] X. Huang and S. Belongie, "Arbitrary style transfer in real-time with adaptive instance normalization," in *Proceedings of the IEEE international conference on computer vision*, 2017, pp. 1501–1510.
- [37] Y. Li, C. Fang, J. Yang, Z. Wang, X. Lu, and M.-H. Yang, "Universal style transfer via feature transforms," in *Advances in neural information processing systems*, 2017, pp. 386–396.
- [38] Y. Li, M.-Y. Liu, X. Li, M.-H. Yang, and J. Kautz, "A closed-form solution to photorealistic image stylization," in *Proceedings of the European conference on computer vision (ECCV)*, 2018, pp. 453–468.
- [39] J. Yoo, Y. Uh, S. Chun, B. Kang, and J.-W. Ha, "Photorealistic style transfer via wavelet transforms," in *Proceedings of the IEEE/CVF international conference on computer vision*, 2019, pp. 9036–9045.
- [40] H. Zhang, I. Goodfellow, D. Metaxas, and A. Odena, "Self-attention generative adversarial networks," in *International conference on machine learning*. PMLR, 2019, pp. 7354–7363.
- [41] D. Y. Park and K. H. Lee, "Arbitrary style transfer with style-attentional networks," in *proceedings of the IEEE/CVF conference on computer vision and pattern recognition*, 2019, pp. 5880–5888.
- [42] S. Liu, T. Lin, D. He, F. Li, M. Wang, X. Li, Z. Sun, Q. Li, and E. Ding, "Adaattn: Revisit attention mechanism in arbitrary neural style transfer," in *Proceedings of the IEEE/CVF international conference on computer vision*, 2021, pp. 6649–6658.
- [43] L. Wang, L. Wang, and S. Chen, "Esa-cycleGAN: Edge feature and self-attention based cycle-consistent generative adversarial network for style transfer," *IET Image Processing*, vol. 16, no. 1, pp. 176–190, 2022.
- [44] A. Vaswani, N. Shazeer, N. Parmar, J. Uszkoreit, L. Jones, A. N. Gomez, Ł. Kaiser, and I. Polosukhin, "Attention is All You Need," *Advances in neural information processing systems*, vol. 30, 2017.
- [45] J. Liang, J. Cao, G. Sun, K. Zhang, L. Van Gool, and R. Timofte, "Swinir: Image restoration using swin transformer," in *Proceedings of the IEEE/CVF International Conference on Computer Vision*, 2021, pp. 1833–1844.
- [46] Z. Wang, X. Cun, J. Bao, W. Zhou, J. Liu, and H. Li, "Uformer: A general u-shaped transformer for image restoration," in *Proceedings of the IEEE/CVF Conference on Computer Vision and Pattern Recognition*, 2022, pp. 17 683–17 693.
- [47] Y.-W. Chen and S.-C. Pei, "Domain adaptation for underwater image enhancement via content and style separation," *IEEE Access*, vol. 10, pp. 90 523–90 534, 2022.

- [48] K. Han, A. Xiao, E. Wu, J. Guo, C. Xu, and Y. Wang, "Transformer in transformer," *Advances in neural information processing systems*, vol. 34, pp. 15 908–15 919, 2021.
- [49] S. Fengxue, S. Yanguo, L. Zhenping, W. Yanqi, Z. Nianchao, W. Yuru, and L. Ping, "Image and video style transfer based on transformer," *IEEE Access*, vol. 11, pp. 56 400–56 407, 2023.
- [50] Y. Jiang, S. Chang, and Z. Wang, "Transgan: Two pure transformers can make one strong gan, and that can scale up," *Advances in Neural Information Processing Systems*, vol. 34, pp. 14 745–14 758, 2021.
- [51] J. Fu, J. Liu, H. Tian, Y. Li, Y. Bao, Z. Fang, and H. Lu, "Dual attention network for scene segmentation," in *Proceedings of the IEEE/CVF conference on computer vision and pattern recognition*, 2019, pp. 3146–3154.
- [52] C.-T. Lin, S.-W. Huang, Y.-Y. Wu, and S.-H. Lai, "Gan-based day-to-night image style transfer for nighttime vehicle detection," *IEEE Transactions on Intelligent Transportation Systems*, vol. 22, no. 2, pp. 951–963, 2020.
- [53] W. Qian, H. Li, and H. Mu, "Circular lbp prior-based enhanced gan for image style transfer," *International Journal on Semantic Web and Information Systems (IJSWIS)*, vol. 18, no. 2, pp. 1–15, 2022.
- [54] K. Xu, L. Wen, G. Li, H. Qi, L. Bo, and Q. Huang, "Learning self-supervised space-time cnn for fast video style transfer," *IEEE Transactions on Image Processing*, vol. 30, pp. 2501–2512, 2021.
- [55] F. Banterle, "Inverse tone mapping," Ph.D. dissertation, Banterle, 2009.
- [56] D. Ulyanov, A. Vedaldi, and V. Lempitsky, "Deep image prior," in *Proceedings of the IEEE conference on computer vision and pattern recognition*, 2018, pp. 9446–9454.
- [57] E. P. Lafortune, S.-C. Foo, K. E. Torrance, and D. P. Greenberg, "Non-linear approximation of reflectance functions," in *Proceedings of the 24th annual conference on Computer graphics and interactive techniques*, 1997, pp. 117–126.
- [58] B. K. Horn and B. G. Schunck, "Determining optical flow," *Artificial intelligence*, vol. 17, no. 1-3, pp. 185–203, 1981.
- [59] K. He, J. Sun, and X. Tang, "Single Image Haze Removal using Dark Channel Prior," *IEEE Transactions on Pattern Analysis and Machine Intelligence*, vol. 33, no. 12, pp. 2341–2353, 2010.
- [60] W. Zhao, J. Zhu, J. Huang, P. Li, and B. Sheng, "Gan-based multi-decomposition photo cartoonization," *Computer Animation and Virtual Worlds*, vol. 35, no. 3, p. e2248, 2024.
- [61] N. Ahn, P. Kwon, J. Back, K. Hong, and S. Kim, "Interactive cartoonization with controllable perceptual factors," in *Proceedings of the IEEE/CVF Conference on Computer Vision and Pattern Recognition*, 2023, pp. 16 827–16 835.
- [62] M. Chen, X. Yu, J. Zhang, and J. Ma, "Decogan: Photo cartoonization based on deformation consistency gan," in *International Conference on Intelligent Computing*. Springer, 2024, pp. 111–121.
- [63] X. Li, W. Zhang, T. Shen, and T. Mei, "Everyone is a cartoonist: Selfie cartoonization with attentive adversarial networks," in *2019 IEEE international conference on multimedia and expo (ICME)*. IEEE, 2019, pp. 652–657.
- [64] H. Wu, Y. Li, X. Liu, C. Li, and W. Wu, "Deep texture cartoonization via unsupervised appearance regularization," *Computers & Graphics*, vol. 97, pp. 99–107, 2021.
- [65] T.-J. Fu, X. E. Wang, and W. Y. Wang, "Language-driven artistic style transfer," in *European Conference on Computer Vision*. Springer, 2022, pp. 717–734.
- [66] J. Zhang and Y. Jiang, "Style transfer technology of batik pattern based on deep learning," *Journal of Fiber Bioengineering and Informatics*, vol. 16, no. 1, pp. 75–85, 2023.
- [67] B. Kim, V. C. Azevedo, M. Gross, and B. Solenthaler, "Transport-based neural style transfer for smoke simulations," *arXiv preprint arXiv:1905.07442*, 2019.
- [68] Z. Lin, Z. Wang, H. Chen, X. Ma, C. Xie, W. Xing, L. Zhao, and W. Song, "Image style transfer algorithm based on semantic segmentation," *IEEE Access*, vol. 9, pp. 54 518–54 529, 2021.
- [69] C. Zheng, H. Li, Y. Ge, Y. He, M. Zhu, H. Sun, J. Kong *et al.*, "Retinal vessel segmentation based on multi-scale feature and style transfer," *Mathematical Biosciences and Engineering*, vol. 21, no. 1, pp. 49–75, 2023.
- [70] W. Ye, C. Liu, Y. Chen, Y. Liu, C. Liu, and H. Zhou, "Multi-style transfer and fusion of image's regions based on attention mechanism and instance segmentation," *Signal Processing: Image Communication*, vol. 110, p. 116871, 2023.
- [71] L.-C. Chen, G. Papandreou, I. Kokkinos, K. Murphy, and A. L. Yuille, "Deeplab: Semantic image segmentation with deep convolutional nets, atrous convolution, and fully connected crfs," *IEEE transactions on pattern analysis and machine intelligence*, vol. 40, no. 4, pp. 834–848, 2017.
- [72] H. Wang, H. Xiong, and Y. Cai, "Image localized style transfer to design clothes based on cnn and interactive segmentation," *Computational Intelligence and Neuroscience*, vol. 2020, no. 1, p. 8894309, 2020.
- [73] H. Madokoro, K. Takahashi, S. Yamamoto, S. Nix, S. Chiyonobu, K. Saruta, T. K. Saito, Y. Nishimura, and K. Sato, "Semantic segmentation of agricultural images based on style transfer using conditional and unconditional generative adversarial networks," *Applied Sciences*, vol. 12, no. 15, p. 7785, 2022.
- [74] B. Niu, Y. Ma, and Y. Qi, "Style transfer of image target region based on deep learning," in *2021 6th International Symposium on Computer and Information Processing Technology (ISCRIPT)*. IEEE, 2021, pp. 486–489.
- [75] S. Yamaguchi, T. Kato, T. Fukusato, C. Furusawa, and S. Morishima, "Region-based painting style transfer," in *SIGGRAPH Asia 2015 Technical Briefs*, 2015, pp. 1–4.
- [76] K. Krutharth and M. Madhavan, "Region-based random color highlighting in artistic style transfer using cnn," in *International Conference on Advances in Electrical and Computer Technologies*. Springer, 2021, pp. 81–90.
- [77] Y.-S. Liao and C.-R. Huang, "Semantic context-aware image style transfer," *IEEE Transactions on Image Processing*, vol. 31, pp. 1911–1923, 2022.



- [78] Z. Huang, J. Zhang, and J. Liao, "Style mixer: Semantic-aware multi-style transfer network," in *Computer Graphics Forum*, vol. 38, no. 7. Wiley Online Library, 2019, pp. 469–480.
- [79] H. Zhang and K. Dana, "Multi-style generative network for real-time transfer," in *Proceedings of the European Conference on Computer Vision (ECCV) Workshops*, 2018, pp. 0–0.
- [80] Y. Yu, D. Li, B. Li, and N. Li, "Multi-style image generation based on semantic image," *The Visual Computer*, vol. 40, no. 5, pp. 3411–3426, 2024.
- [81] Y. Fu, Y. Xie, Y. Fu, and Y.-G. Jiang, "Styleadv: Meta style adversarial training for cross-domain few-shot learning," in *Proceedings of the IEEE/CVF Conference on Computer Vision and Pattern Recognition*, 2023, pp. 24 575–24 584.
- [82] Y. Huang, M. He, L. Jin, and Y. Wang, "Rd-gan: Few/zero-shot chinese character style transfer via radical decomposition and rendering," in *Computer Vision–ECCV 2020: 16th European Conference, Glasgow, UK, August 23–28, 2020, Proceedings, Part VI 16*. Springer, 2020, pp. 156–172.
- [83] K. Liu, F. Zhan, Y. Chen, J. Zhang, Y. Yu, A. El Saddik, S. Lu, and E. P. Xing, "Stylerrf: Zero-shot 3d style transfer of neural radiance fields," in *Proceedings of the IEEE/CVF Conference on Computer Vision and Pattern Recognition*, 2023, pp. 8338–8348.
- [84] Q. Cai, M. Ma, C. Wang, and H. Li, "Image neural style transfer: A review," *Computers and Electrical Engineering*, vol. 108, p. 108723, 2023.
- [85] Y. Jing, Y. Yang, Z. Feng, J. Ye, Y. Yu, and M. Song, "Neural style transfer: A review," *IEEE transactions on visualization and computer graphics*, vol. 26, no. 11, pp. 3365–3385, 2019.
- [86] J. Johnson, A. Alahi, and L. Fei-Fei, "Perceptual losses for real-time style transfer and super-resolution," in *Computer Vision–ECCV 2016: 14th European Conference, Amsterdam, The Netherlands, October 11–14, 2016, Proceedings, Part II 14*. Springer, 2016, pp. 694–711.
- [87] D. Ulyanov, A. Vedaldi, and V. Lempitsky, "Instance normalization: The missing ingredient for fast stylization," in *arXiv preprint arXiv:1607.08022*, 2016.
- [88] H. Chen, F. Shao, X. Chai, Y. Gu, Q. Jiang, X. Meng, and Y.-S. Ho, "Quality evaluation of arbitrary style transfer: Subjective study and objective metric," *IEEE Transactions on Circuits and Systems for Video Technology*, vol. 33, no. 7, pp. 3055–3070, 2022.
- [89] X. Wang, W. Wang, S. Yang, and J. Liu, "Clast: Contrastive learning for arbitrary style transfer," *IEEE Transactions on Image Processing*, vol. 31, pp. 6761–6772, 2022.
- [90] Y. Zhang, F. Tang, W. Dong, H. Huang, C. Ma, T.-Y. Lee, and C. Xu, "Domain enhanced arbitrary image style transfer via contrastive learning," in *ACM SIGGRAPH 2022 conference proceedings*, 2022, pp. 1–8.
- [91] E. H. Land and J. J. McCann, "Lightness and retinex theory," *Josa*, vol. 61, no. 1, pp. 1–11, 1971.
- [92] D. J. Jobson, Z. Rahman, and G. A. Woodell, "A Multiscale Retinex for Bridging the Gap between Color Images and the Human Observation of Scenes," *IEEE Transactions on Image processing*, vol. 6, no. 7, pp. 965–976, 1997.
- [93] C. Fabbri, M. J. Islam, and J. Sattar, "Enhancing Underwater Imagery using Generative Adversarial Networks," in *IEEE International Conference on Robotics and Automation (ICRA)*. IEEE, 2018, pp. 7159–7165.
- [94] J. Li, K. A. Skinner, R. M. Eustice, and M. Johnson-Roberson, "Watergan: Unsupervised generative network to enable real-time color correction of monocular underwater images," *IEEE Robotics and Automation letters*, vol. 3, no. 1, pp. 387–394, 2017.
- [95] N. Li, Z. Zheng, S. Zhang, Z. Yu, H. Zheng, and B. Zheng, "The synthesis of unpaired underwater images using a multistyle generative adversarial network," *IEEE Access*, vol. 6, pp. 54 241–54 257, 2018.
- [96] H. Yang, F. Tian, Q. Qi, Q. J. Wu, and K. Li, "Underwater image enhancement with latent consistency learning-based color transfer," *IET Image Processing*, vol. 16, no. 6, pp. 1594–1612, 2022.
- [97] A. Anil, G. Sreelatha *et al.*, "A novel approach for underwater image enhancement using style transfer technique," in *2023 International Conference on Control, Communication and Computing (ICCC)*. IEEE, 2023, pp. 1–6.
- [98] M. E. Fathy, S. A. Mohamed, M. I. Awad, and H. E. Abd El Munim, "Submergestylegan: Synthetic underwater data generation with style transfer for domain adaptation," in *2023 International Conference on Digital Image Computing: Techniques and Applications (DICTA)*. IEEE, 2023, pp. 546–553.
- [99] X. Zhou, C. Yu, S. Yuan, X. Yuan, H. Yu, and C. Luo, "Learning visual representation of underwater acoustic imagery using transformer-based style transfer method," in *Proceedings of the 15th International Conference on Digital Image Processing*, 2023, pp. 1–9.
- [100] L. Yang, B. Kang, Z. Huang, X. Xu, J. Feng, and H. Zhao, "Depth anything: Unleashing the power of large-scale unlabeled data," in *Proceedings of the IEEE/CVF Conference on Computer Vision and Pattern Recognition*, 2024, pp. 10 371–10 381.
- [101] M. J. Islam, S. S. Enan, P. Luo, and J. Sattar, "Underwater Image Super-Resolution using Deep Residual Multipliers," in *IEEE International Conference on Robotics and Automation (ICRA)*. IEEE, 2020, pp. 900–906.
- [102] "Unsplash: Free high-resolution photos," 2024, accessed: August 30, 2024. [Online]. Available: <https://unsplash.com/>
- [103] "Flickr: A comprehensive image sharing platform," 2024, accessed: August 30, 2024. [Online]. Available: <https://www.flickr.com/>
- [104] Y. Peng *et al.*, "Single image haze removal using dark channel prior," in *IEEE Conference on Computer Vision and Pattern Recognition*, 2015, pp. 3210–3217.
- [105] Y. Song *et al.*, "Rapid underwater image enhancement using weighted guided filtering," in *2018 IEEE International Conference on Image Processing*, 2018, pp. 341–345.
- [106] H. Gao, H. Yuan, Z. Wang, and S. Ji, "Pixel transposed convolutional networks," *IEEE transactions on pattern analysis and machine intelligence*, vol. 42, no. 5, pp. 1218–1227, 2019.
- [107] K. O'shea and R. Nash, "An introduction to convolutional neural networks," *arXiv preprint arXiv:1511.08458*, 2015.

- [108] S. Ioffe and C. Szegedy, "Batch normalization: Accelerating deep network training by reducing internal covariate shift," in *International conference on machine learning*. pmlr, 2015, pp. 448–456.
- [109] V. Nair and G. E. Hinton, "Rectified linear units improve restricted boltzmann machines," in *Proceedings of the 27th International Conference on Machine Learning (ICML)*. Omnipress, 2010, pp. 807–814.
- [110] T.-Y. Lin, M. Maire, S. Belongie, J. Hays, P. Perona, D. Ramanan, P. Dollár, and C. L. Zitnick, "Microsoft coco: Common objects in context," in *Computer Vision—ECCV 2014: 13th European Conference, Zurich, Switzerland, September 6-12, 2014, Proceedings, Part V 13*. Springer, 2014, pp. 740–755.
- [111] D. E. Rumelhart, G. E. Hinton, and R. J. Williams, "Learning representations by back-propagating errors," *nature*, vol. 323, no. 6088, pp. 533–536, 1986.
- [112] L. Hong, X. Wang, G. Zhang, and M. Zhao, "Usod10k: a new benchmark dataset for underwater salient object detection," *IEEE transactions on image processing*, 2023.
- [113] X. Xu, S. Xu, L. Jin, and E. Song, "Characteristic analysis of otsu threshold and its applications," *Pattern recognition letters*, vol. 32, no. 7, pp. 956–961, 2011.
- [114] K. He, J. Sun, and X. Tang, "Guided image filtering," *IEEE transactions on pattern analysis and machine intelligence*, vol. 35, no. 6, pp. 1397–1409, 2012.
- [115] Y. Deng, C. Liu, X. Zhu, J. Zhang, and C. C. Loy, "StyTr<sup>2</sup>: Image style transfer with transformers," in *Proceedings of the IEEE/CVF Conference on Computer Vision and Pattern Recognition (CVPR)*, 2021, pp. 11 369–11 378.
- [116] Z. Qi *et al.*, "Artistic style transfer with internal-external learning and contrastive learning," *arXiv preprint arXiv:2009.12335*, 2020.
- [117] T. Chai and R. R. Draxler, "Root mean square error (rmse) or mean absolute error (mae)?—arguments against avoiding rmse in the literature," *Geoscientific Model Development*, vol. 7, no. 3, pp. 1247–1250, 2014.
- [118] Z. Wang, A. C. Bovik, H. R. Sheikh, E. P. Simoncelli *et al.*, "Image Quality Assessment: from Error Visibility to Structural Similarity," *IEEE Transactions on Image Processing*, vol. 13, no. 4, pp. 600–612, 2004.
- [119] W. Xue, L. Zhang, X. Mou, and A. C. Bovik, "Gradient magnitude similarity deviation: A highly efficient perceptual image quality index," *IEEE Transactions on Image Processing*, vol. 23, no. 2, pp. 684–695, 2014.
- [120] R. Zhang, P. Isola, A. A. Efros, E. Shechtman, and O. Wang, "The unreasonable effectiveness of deep features as a perceptual metric," in *Proceedings of the IEEE conference on computer vision and pattern recognition*, 2018, pp. 586–595.
- [121] R. R. Selvaraju, M. Cogswell, A. Das, R. Vedantam, D. Parikh, and D. Batra, "Grad-cam: Visual explanations from deep networks via gradient-based localization," in *Proceedings of the IEEE international conference on computer vision*, 2017, pp. 618–626.
- [122] E. Reinhard, M. Adhikhmin, B. Gooch, and P. Shirley, "Color transfer between images," *IEEE Computer graphics and applications*, vol. 21, no. 5, pp. 34–41, 2001.
- [123] C. Li, C. Guo, W. Ren, R. Cong, J. Hou, S. Kwong, and D. Tao, "An underwater image enhancement benchmark dataset and beyond," *IEEE Transactions on Image Processing*, vol. 29, pp. 4376–4389, 2020.
- [124] A. Duarte, F. Codevilla, J. D. O. Gaya, and S. S. Botelho, "A dataset to evaluate underwater image restoration methods," in *OCEANS 2016-Shanghai*. IEEE, 2016, pp. 1–6.
- [125] A. Abdullah, T. Barua, R. Tibbetts, Z. Chen, M. J. Islam, and I. Rekleitis, "CaveSeg: Deep Semantic Segmentation and Scene Parsing for Autonomous Underwater Cave Exploration," in *IEEE International Conference on Robotics and Automation (ICRA)*. IEEE, 2024.
- [126] T. Porto Marques and A. Branzan Albu, "L2uwe: A framework for the efficient enhancement of low-light underwater images using local contrast and multi-scale fusion," in *Proceedings of the IEEE/CVF Conference on Computer Vision and Pattern Recognition Workshops*, 2020, pp. 538–539.
- [127] G. Hinton, O. Vinyals, and J. Dean, "Distilling the knowledge in a neural network," *arXiv preprint arXiv:1503.02531*, 2015.
- [128] C. Ancuti, C. O. Ancuti, T. Haber, and P. Bekaert, "Enhancing underwater images and videos by fusion," in *2012 IEEE conference on computer vision and pattern recognition*. IEEE, 2012, pp. 81–88.
- [129] Y. Y. Schechner and N. Karpel, "Recovery of underwater visibility and structure by polarization analysis," *IEEE Journal of oceanic engineering*, vol. 30, no. 3, pp. 570–587, 2005.
- [130] A. K. Aggarwal, "Fusion and enhancement techniques for processing of multispectral images," *Unmanned aerial vehicle: applications in agriculture and environment*, pp. 159–175, 2020.
- [131] T. Park, M.-Y. Liu, T.-C. Wang, and J.-Y. Zhu, "Semantic image synthesis with spatially-adaptive normalization," in *Proceedings of the IEEE/CVF conference on computer vision and pattern recognition*, 2019, pp. 2337–2346.